UNIVERSITY OF CAMBRIDGE

Investigating the Deformation Mechanisms beneath Shallow Foundations

By
Srikanth Madabhushi (T)

Fourth-year Undergraduate Project in Group D, 2013/2014

I hereby declare that, except where specifically indicated, the work submitted herein is my own original work

Signed: Date:

Acknowledgements

I would like to thank my supervisor Dr Stuart Haigh for his continued help and insight into both the practical and analytical aspects of the project. The assistance of the Schofield centre technicians was also invaluable. Special thanks must go to Mr Richard Adams and Mr Kristian Pether for their practical assistance, and Mr John Chandler for his advice and practical solutions. Finally, the Schofield centre researchers support and patience in showing me the ropes was also greatly appreciated, in particular the advice from Dr Charles Heron, Ms. April Bowman and Mr Peter Kirkwood.

Investigating the Deformation Mechanisms beneath Shallow Foundations

Srikanth Madabhushi – Trinity College

2013/2014

Technical Abstract

Shallow foundations are used to support small to medium sized structures around the globe. The loads from the structure are spread over a larger area; hence the stresses induced in the soil are reduced. The globally wide spread use of shallow foundations means the optimisation between safety, performance and efficiency can have large scale ramifications in terms of socio-economic and environmental costs.

Historically, design of shallow foundations has involved calculating the ULS load that may be applied, and reducing this load by a specified factor to limit the ground movements and hence superstructure settlements. The factors used are often based solely on professional judgment and industry experience, without necessarily having an underlying theoretical basis.

In an era where both environmental and fiscal drivers necessitate a move away from 'overly conservative' design, satisfying the SLS requirements through arbitrarily scaling down the ULS loads is becoming increasingly difficult to justify. A more rationalised design approach for shallow foundations was initially proposed by McMahon et al (2013a) and served as the catalyst for this project. McMahon et al (2013a) discovered that the deformation mechanism may change depending on the level of loading or settlement. Accurate knowledge of the soil movements facilitates calculation of the load-settlement behaviour through the application of upper bound analyses.

In this work, the visualisation of the deformation mechanisms beneath both circular and strip shallow foundations was successfully achieved using the GeoPIV software. The deformation mechanism was observed to change as the footing was loaded up to the ULS, agreeing well with previous observations from McMahon et al (2013a) for circular footings. Additional experiments under plane strain soil conditions revealed

similar results for strip footings. Though the pattern of mechanisms was similar, the rate of change of mechanisms was noted to be faster for the circular footing.

The mechanisms appeared to change almost continuously. There was an initial 'elastic' mechanism in which small, vertically downwards movements of a large amount of the soil mass accommodated the footing displacement with minimal 'heaving' at the soil surface. It was noted that this implies the soil was not behaving in a perfectly undrained manner, but it was also acknowledged that this would not be true in practice either. As the footing displacement increased, soil near the edges of the foundation moved horizontally outwards as well as vertically downwards. This can be well approximated by the cavity expansion model proposed by McMahon et al (2013a). At very large footing displacements (induced by loads above the usual design working loads of the footings) a 'Prandtl+' mechanism develops, in which the three zones predicted by Prandtl can be clearly identified as well as small movements of soil outside these regions.

Upper bound analyses provided further insight into the project, allowing comparison between the experimentally observed load-settlement behaviour and theoretically derived fields. The best match between the experimentally measured results and theoretical fields was achieved by mixing the elastic solution with the Osman field for circular foundations and the pure Prandtl field for the strip foundations. The proportions of elastic field in the optimum mixes reflected the differing rate of change of deformation mechanisms beneath circular and strip foundations observed in the experimental results.

The practical implications of these findings may be profound. The changing deformation mechanism affects the load required to induce a given footing displacement. It was found that under typical 'working loads' for the footing the deformation mechanism is not well described by either purely elastic or purely plastic fields. This project highlights that the knowledge of the changing deformation mechanism is necessary in order to accurately predict the settlement of the foundation at the working loads.

Such methods may allow for increasingly technically justified designs of shallow foundations of the future which can strike the balance between efficiency and safety that is required of the modern Geotechnical Engineer.

Contents

1 Introduction

The use of shallow foundations to support small to medium sized structures is globally prolific. In essence, shallow foundations spread the load of the structure over a larger area, and hence reduce the stresses imposed on the soil. Their use in practice around the world is due to their relatively low costs and speed of design and construction.

The design of such foundations is typically based on Ultimate Limit State (ULS) calculations. Plasticity theory is employed to find the maximum load which may be applied before 'failure'. We can define the ULS to be the limiting applied load before a loss of equilibrium or stability. The other crucial limit state in structural design is the Serviceability Limit State (SLS). Loss of utility through excessive deformations or differential ground settlements, and hence induced strains in the structure, is estimated to be the leading cause of unsatisfactory building performance. This is particularly an issue for usual construction materials such as masonry or concrete, owing to their brittle behaviour. Typically, shallow foundation design has employed 'partial safety factors' on the ULS collapse load in an attempt to control the ground settlements. The factors used are often based solely on professional judgment and industry experience, without necessarily having an underlying theoretical basis.

The balance between structural safety and robustness against the economic cost of inefficient design is become increasingly critical. In an era where both environmental and fiscal drivers necessitate a move away from 'overly conservative' design, the need to rationalise design decisions is a growing imperative. To this end, recent research on shallow foundations has concentrated on designing shallow foundations from a SLS viewpoint, focussing particularly on linking the applied load to the soil movements. It is important early on to draw a distinction between a deformation mechanism and a failure mechanism. Describing the overall displacements of the soil at ULS defines the failure mechanism. Prior to loading at the ULS, the soil will naturally displace in response to loading, and such displacements describe the deformation mechanism. It is not necessary that the deformation mechanism and the ultimate failure mechanism are the same. The deformation mechanism is inherently linked to the SLS, as the movement of the soil under the working loads governs the settlement of the superstructure in service.

Recent work by McMahon et al (2013a) has led to the discovery that the deformation mechanism may change depending on the level of loading or settlement. Accurate knowledge of the soil movements facilitates calculation of the settlement of the superstructure with the applied load. The ability to calculate the generalised load-settlement behaviour of shallow foundations would provide the framework for a far more robust design methodology than currently used. The crux of the issue for current design is not only that scaling down the ULS to meet the SLS is not theoretically justified. Rather, it is additionally the fact that the designer has no way of knowing where the final design lies between the extremes of 'too conservative' and the limit state. A factor of safety that is excessive at some sites can potentially lead to failure at others.

The motivation and aims for this project can be summarised as follows:

- Gather experimental evidence of the changing mechanisms observed by McMahon et al (2013), with a view to confirming analytical and finite element predictions found in literature
- Research to date has often been either purely theoretical or reports of measured behaviour. The novel aspect of this work is to attempt to marry together the experimentally measured and theoretically calculated load-settlement behaviour
- Confirmation of the changing mechanisms and predictive models in literature may have profound implications for the future design of shallow foundations. Accurate and reliable predictions of settlement of shallow foundations, given the loading conditions can facilitate a more robust design method than that currently employed
- This could lead to potentially safer design where previous arbitrary factors of safety have been misapplied or more efficient design where the factors have been too conservative

2. Literature Review

When considering research into shallow foundation failure, there are numerous approaches which may be taken to investigate the problem. We may consider the ultimate bearing capacity, i.e. the maximum load that may be applied to a footing before 'collapse'. However, settlements of the foundation warrant equal care, as, notwithstanding serviceability considerations, these may also induce ultimate limit state failure of the supported superstructure. The settlements can be understood through investigation of the deformation mechanism suffered by the soil. This in turn may be studied through analytical predictions, experimental measurements or finite element analyses. Traditionally, elastic solutions have been employed to ascertain the load displacement behaviour. However, recent work has concentrated on more accurate modelling the stress-strain behaviour of the soil.

Throughout such studies a view to the practical application of the knowledge must be maintained. The use of shallow foundations to support small structures globally is prolific, and hence, the ability to make accurate and informed predictions of the settlement is critical. The following literature review will concentrate on work pertaining specifically to shallow foundations on clayey soils in the 'short term'. It is worth pointing out that undrained conditions can dominate the early design life of shallow foundations on most clays. Further, the undrained capacity will be critical for the design involving normally or lightly consolidated clays, which tend to shear harden.

2.1 Historical Perspective

In 1921 Prandtl published his work on the penetrative resistance of 'plastic building materials'. The results were derived using Airy stress functions to satisfy both equilibrium and material laws. Terazaghi (1943) applied these solutions to the case of shallow foundations on soil.

Terazaghi's solutions can also be obtained using a lower and upper bound approach based on plasticity theory. By performing the appropriate Mohr's circle analysis or work calculation for the lower bound or upper bound solutions respectively, the same bearing capacity factor for the footing can be obtained. The implication is that for an undrained soil mass with a constant undrained shear strength and no surcharge, the 'true solution' has been found, provided one can model the soil as rigid perfectly plastic. This 'true solution' gives the bearing capacity factor (ratio of failure stress to the undrained shear strength) given in Equation 2.1.

$$N_c = \frac{\sigma_{failure}}{s_u} = 2 + \pi \qquad \text{Equation 2-1}$$

However, soil is often described as highly non-linear, even at small shear strains. Hence, whether the clayey soil is normally consolidated or over consolidated, its behaviour is not well captured by the assumption of a rigid-perfectly plastic material. This is especially true at small shear strains, and typically designs in practice would aim to prevent the development of large shear strains.

Although modifications to account for embedment depth (Skempton, 1951), vertical and moment loading (Meyerhof, 1953) or vertical and horizontal loading (Green, 1954) exist, the fundamental calculation for the ultimate limit state of a shallow foundation under undrained conditions is based directly on Prandtl's and Terzaghi's work. Eurocode 7 states that at this calculated ULS loading level, there will be 'considerable deformation'. One proposed approach is to apply a factor of safety of between 2 and 3 to this maximum load in order to limit settlements. This factor is based on professional experience and there is no theoretical basis that suggests scaling the ULS will meet the SLS criteria. As discussed earlier, the issue with such factors is that the 'level of conservativeness' is not actually known, and further that the factors must be varied from site to site based solely on professional judgement.

Boussinesq's (1885) elastic solution for a vertical point load on a half space is an example of early work that can be used to design for the SLS. His solution was later integrated by Skemptom and Bjerrum (1957), essentially producing a load-settlement prediction. However, Osman and Bolton (2005) argue that linear elasticity (whilst preferable to a rigid perfectly plastic soil model) is a poor way to calculate settlement. This led to the concept of 'Mobilisable Strength Design' (MSD). The underlying theory is as follows. It is well known that stresses are induced by loads and strains by displacements, hence the load-settlement behaviour may be inferred from a suitably scaled stress- strain curve.

Gourvenec and Mana (2011) detail the historical use of Finite Element (FE) analysis, Finite Element Limit Analysis (FELA) and the 'Method of characteristics' to assess the undrained vertical bearing capacity of shallow foundations from 1951 to 2011. Comparisons are made between methods and attempts to rationalise the disparities between upper and lower bound solutions. However, this is done mainly in the context of the ultimate bearing capacity (for ULS design), rather than using FE or FELA methods to predict the load displacement behaviour (i.e. for SLS design).

2.2. Precursor to this project

McMahon et al (2013a) conducted centrifuge experiments in order to observe the mechanism beneath circular shallow foundations on clay. Strong evidence was gathered to suggest that the deformation mechanism changed depending on the loading. At high loads and settlements the observed deformation mechanism did agree well with the Prandtl deformation mechanism. However, at lower loads and settlements the observed displacement of the soil was described as resembling an 'ellipsoidal cavity expansion'. Examples of the different mechanisms observed are illustrated in Figure 2-1.

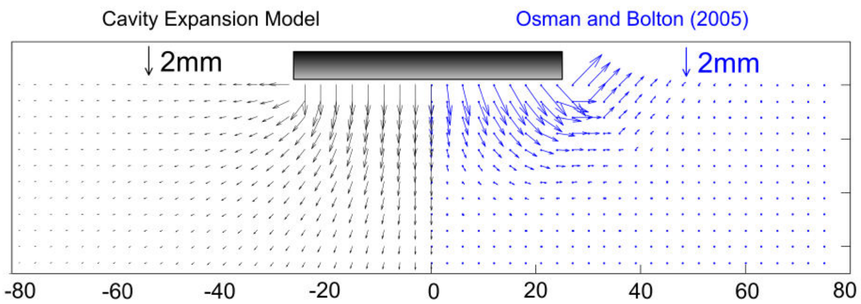

Figure 2-1: Comparison of deformation mechanisms following from McMahon et al (2013a)

This work was extended in McMahon et al (2013b). Using various deformation mechanisms, upper bound analyses were conducted to predict the load settlement behaviour based on the energy dissipated in the soil. It was found that the 'optimal mechanism' (lowest work done to cause failure) switched as the settlement increased. This agreed well with the experimental observations of changing mechanisms. Further, the behaviour predicted by the optimal mechanism at various settlements matched well with the results of finite element analyses in literature, by Gourvenec and Randolph (2002) or Taiebat and Carter (2010) for example.

The implication of these findings for design is summarised in McMahon et al (2013a). A single design line for predicting the footing displacement given the applied load was proposed. This design line was independent of the undrained shear strength of the soil and its stiffness.

The work by McMahon et al (2013a,b) will be discussed in more detail when the experimental results are further discussed and analysed in Section 5.2. Further research in this area by Klar and Osman (2008) will also be introduced in that section.

We may conclude the literature review with the following key points:

- The ultimate bearing capacity of shallow foundations is well understood for a variety of soil and loading conditions, through both theoretical derivations and analytical/numerical analyses
- However, until relatively recently, research into the serviceability limit state which accounts for the true non-linear stress strain behaviour of soil has been sparse
- Work by McMahon et al (2013) has focussed on determining the load-settlement behaviour for design by understanding the soil deformation mechanisms. Upper bound predictions of load-settlement behaviour can be constructed through consideration of the energy dissipated by the mechanism
- Whilst this is reinforced by results from finite element analyses, substantial experimental data to verify such changes of mechanism, or even to identify the mechanism at intermediate settlements, is lacking
- The novel aspect of the work presented in this report will concentrate on linking the experimentally measured load-settlement behaviour to the analytically derived equivalent.

3. Experimental Work

3.1 Scope of Experimental Work

The first aim of this project was to gather further experimental evidence for the changing deformation mechanism observed beneath shallow foundations in undrained conditions on clayey soils. The experimental work in this project employed small scale model tests at '1 g' rather than using a centrifuge. Two foundation types were considered. Firstly, circular foundations which are axisymmetric in terms of both deformation and strains, and which were investigated by McMahon et al (2013a) were tested. These are commonly used beneath circular piers for bridges or columns etc. Secondly, strip foundations were considered, which induce plane strain conditions, and are commonly used for supporting load bearing walls etc. The visualisation of the deformation mechanism will be achieved using the Particle Image Velocimetry (PIV) technique that is explained in Section 3.2.6.

By conducting the tests in this project at 1 g, one is afforded various advantages. A common criticism of small scale tests is that due to the non-linear, stress-dependent nature of soils, the observed behaviour at small scale and hence at low effective stresses cannot be easily related to field scale behaviour. However, in the ensuing tests the soil was loaded with a large overburden pressure during consolidation to increase its shear strength. As this was removed before testing, the clay experiences large suctions and hence correspondingly large effective stresses at the time of testing. An even bigger advantage of small scale testing for this project is the relative ease with which soil of uniform undrained shear strength can be produced. Due to the self-weight of layers of clay increasing with depth, centrifuge tests invariably produce a shear strength profile that increases with depth. This is not accounted for in most of the theoretical formulations described in the Literature Review, and hence the small scale tests carried out reflect the analytical models being verified more accurately than previous experimental work.

In order to predict the load settlement behaviour for different soils, McMahon et al (2013) normalise the theoretically predicted settlement with the ratio of the shear modulus (G) to the undrained shear strength (S_u). Hence, in order to compare the experimental results from this project in a similar fashion, experimental determination of these values was required. This will be described in Section 3.2.8.

3.2 Experimental Design and Procedure

Following from Section 3.1, the following apparatus and methods were used to collect the required data. Throughout this section, the experimental accuracy will also be discussed.

3.2.1 Clay consolidation

The clay used in the experiments was constituted from slurry. This was in order to reduce the risk of soil strength and stiffness anisotropy as far as possible. E-grade Kaolin clay was used, which compared to other grade clays is quicker draining hence consolidates faster. A water content of 100% was used for the slurry, with the excess water drained from the top and bottom of the consolidometer as the clay was loaded. The mass of clay required was inferred from the volume of the testing tank, back calculating the initial specific volume along the 'λ line' from the final required stress. The final required stress was taken to be five times the required undrained shear strength, following Vardanega and Bolton (2012).

Figure 3-1: Automatic Consolidometer and testing tank used

Whilst it is not expected this would produce exactly the nominal undrained shear strength specified, for the purposes of this experiment it was more important that the three batches tested had different soil properties, and that these properties could be accurately determined.

The consolidometer (presented in Figure 3-1) applies a set load via a hydraulic piston. The loading was increased in increments to prevent the clay from being squeezed out around the piston edges. Once no further settlement was observed, the piston was unloaded in increments to prevent air entry into the clay.

3.2.2 Foundation Design

The internal dimensions of the testing tank (pictured in Figure 3-1) were 200 × 788 × 440 mm. For these fixed dimensions, the footing sizes were designed. Larger footings were preferred to allow easier visualisation of the deformation mechanisms and facilitate easier instrumentation and connections to the footings. At least two footings were to be tested in each batch of consolidated clay, and the need to avoid boundary effects limited the size of footings that could be used.

For purely semi-circular displacements below the footing (i.e. approximately elastic displacements) and by conserving volume, an approximate 'radius of influence' for a strip footing was defined. It was calculated that for a footing width of 50 mm, a 5 mm footing displacement implies a displacement of 0.4 mm at a radius of 200 mm (a quarter of the tank width). Larger footing displacements are very unlikely to result in an elastic field (and the more likely Prandtl field of deformations occurs within 1.5 footing widths, i.e. 75 mm) hence the final strip footing design had a width of 50 mm. A circular footing induces deformation in 3 dimensions and hence has a smaller extent, so a circular footing diameter of 50 mm was also deemed acceptable.

In order to allow visualisation of the deformation mechanism, a semi-circular foundation flush with the Perspex was used. Using a semi-circle to represent a circular footing is valid for axisymmetric conditions. The strip footing length of 198 mm was chosen so the total length (including a layer of PTFE to prevent scratches) allowed the foundation to sit flush with the Perspex front of the tank. This was

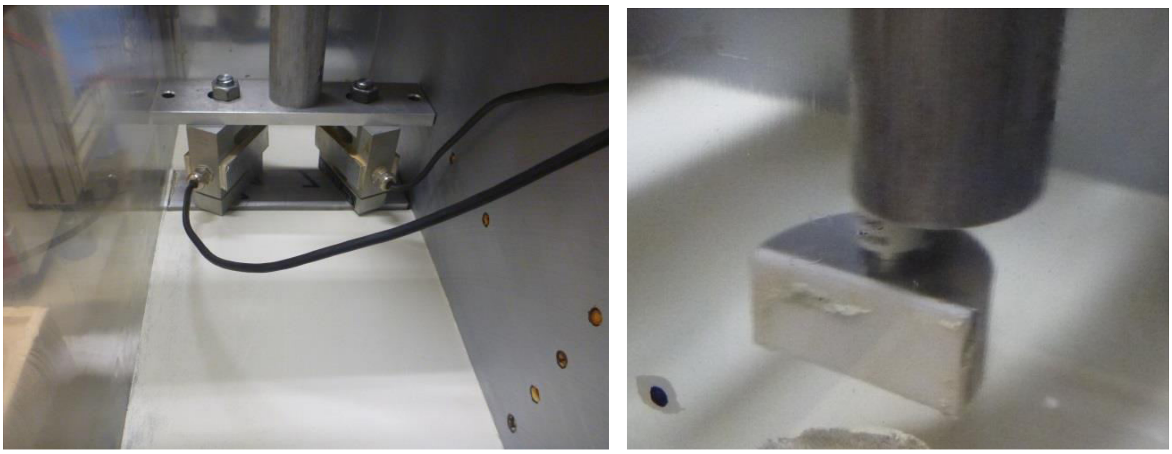

Figure 3-2: Final designs of Strip Footing (left) and Semi-Circular Footing (right) used in experiments

required for the soil movement tracking software to function. Both the strip footing and semi-circular footing had thicknesses of 20 mm. This was the standard plate thickness that the foundations were manufactured from. Deflections of the strip footing were calculated using a simply supported beam with a distributed load equal to $5.14bS_u$ (i.e. the ULS stress times the footing width) idealisation, and were found to be negligible. The self-weight of the larger footing (the strip footing made from aluminium) is less than 0.5 % of the ULS bearing capacity. Figure 3-2 shows the final foundation design used in the experiments.

3.2.3 Foundation Instrumentation

Figure 3-2 also illustrates the load cells used to measure the applied foundation loads. The strip footing had two 'S shaped' load cells in parallel and the semi-circular footing had a single miniature diaphragm load cell. These were installed in series between the foundation and actuator arm (see Section 3.2.5), in order to measure the load applied to the foundation. The load cells selected represented a trade-off between sensitivity to changes at small applied loads and being able to withstand the maximum ULS capacity of the foundations (based on the Prandtl solution). As shown in Figure 3-2, the strip footing load cells were rigidly bolted between the strip foundation and a connecting plate. This helped prevent vertical deflections of the footing. Miniature diaphragm load cells are very sensitive to moment loading. During calibration of the instruments it was discovered a 0.5 Nm of moment loading affected the uniaxial load calibration factor for the miniature diaphragm load cell by as much as 40 %. In order to minimise this effect, the load cell was installed such that it was flush with the footing and actuator arm, using washers as shown in Figure 3-2. Further, the footings were intended to displace vertically downwards following the face of the Perspex, and hence the moments induced in the load cell should have been minimal.

Figure 3-3: LVDT setup

At the top of the actuator arm a linear variable differential transformer (LVDT) was used to record displacement of the actuator, and hence footing. The setup is presented in Figure 3-3. A LVDT was selected over using a draw wire potentiometer due to its higher accuracy (±0.01 mm vs ±1 mm) and easier installation. Calibration of the load cells and LVDT will be discussed in the following section.

3.2.4. Data acquisition and Calibration

In order to read and record the signals from the instruments detailed above, the signals were first amplified using a junction box and interfaced with a computer using the DASYLAB 9.0 data acquisition software. The instruments produce voltages proportional to the physical input, i.e. strains in the case of the load cells (typically a Wheatstone bridge is used to precisely find the change in resistance, and indicating the applied strains and hence loads) or displacement in the case of the LVDT. Calibration is required to convert these voltage changes back into the physical change. Load cells were calibrated by applying known weights and measuring the change in voltage. Similarly, the LVDT was calibrated by precisely applying displacements using an electronic micrometer and measuring the voltage changes. These produce graphs of the physical input vs. the instrument signal. The function from the best fit line can then be used to convert the voltage signal from the experimental data.

Load cells and LVDT's typically remain linear in their recommended usage range, as illustrated by Figure 3-4. In terms of accuracy, the load cells and LVDT used can theoretically produce measurements accurate to ±0.01 N and ±0.01 mm respectively. However, in practice this is often somewhat reduced by the noise in the signal, either from the connecting cables, junction box or data acquisition software. Standard low pass filters were hence used to filter the recorded data.

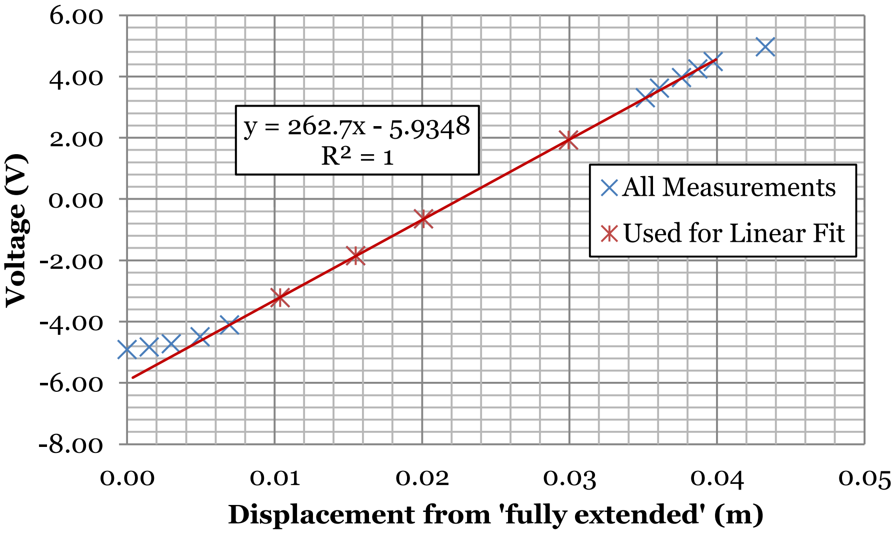

Figure 3-4: Example of calibration curve for a LVDT

3.2.5. 1D Actuator

The footings were driven into the clay using a 1D actuator (shown in Figure 3-5). The 1D Actuator is a single geared actuator which, for a given voltage, current and dial setting, drives the actuator arm at a constant velocity. A constant velocity actuator was preferred for this experiment rather than a constant force actuator, as the force to drive the footing increases as it displaces. The driving velocity was selected to be 0.1 mm s^{-1} for all experiments.

Figure 3-5: 1D Actuator

As slow a velocity as possible was selected in order to improve the visualisation of the deformation mechanism. The assumption that the soil remains undrained for even the slowest driving velocity will be examined in the discussion of results.

3.2.6. Visualising the deformation mechanism

The visualisation of the soil movements was achieved by employing the method of Particle Image Velocimetry (PIV).

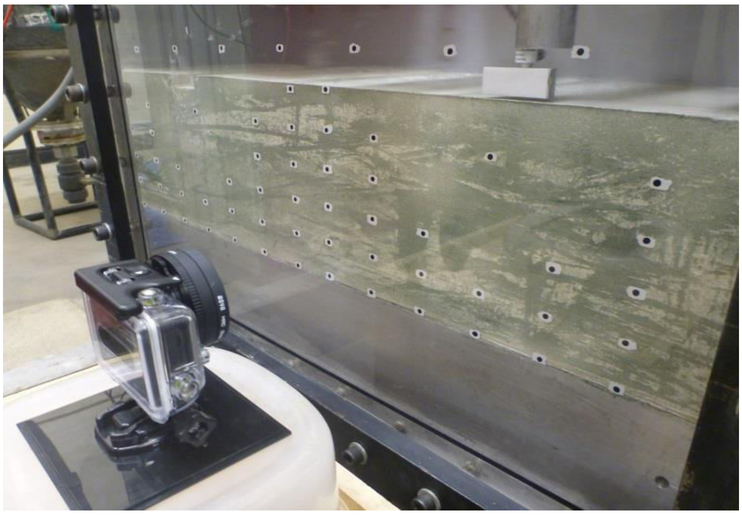
Figure 3-6: Illustration of 'texturing' used on clay

The theory behind PIV (applied to tracking soil movements) is that for a given picture of a soil plane, a sufficiently high resolution camera allows a number of discrete patches across the picture to be uniquely distinguished, based on the unique spatial variation of colour intensity across the patch. In a subsequent picture the patches may move but the unique intensity distribution of each patch still allows them to be identified. Hence, as soil movements are induced each of the patches movements can be recorded, allowing for a displacement field of the soil body to be generated with time. The higher the resolution of the camera and the smaller the soil displacements between frames (achieved by either loading slowly or using a high frames per second camera) the better the tracking of soil movements will be.

The specific PIV software used in this experiment was the GeoPIV software (implemented in MATLAB) written by White & Take (2002). The use of this software to accurately track soil movements has become a relatively standardised procedure, and hence only the particularly relevant aspects for the experiments carried out will be discussed in the following text. A fuller discussion of the methodology and accuracy of the GeoPIV software can be found in White et al (2003).

In order to track the movements of the Kaolin clay behind the Perspex window, 'texturing' needed to be added in order to allow the software to identify unique patches. This was achieved by applying a fine layer of Hostun sand mixed with blue dye to the clay face behind the Perspex window. This is pictured in Figure 3-6. The front of the Perspex is greased in order to limit the affect the textured layer has on the clay behaviour.

These steps allow the software to track the relative displacements of the soil in 'pixel space'. In order to find the magnitude of these recorded displacements in terms of millimetres, 'control markers' were used. These are fixed points of reference between frames, and are the black permanent marker circles against a white background seen in Figure 3-6. The software calibrates the displacements against the spacing between these control markers. The spacing between control markers is itself precisely determined by using a grid of reference dots with precisely measured spacing. These are often printed on Mylar sheets to prevent thermal distortions of the spacing. White et al (2003) describe how this procedure can result in tracking of displacements to sub-pixel accuracy.

In general, the greater the number of control markers the greater the accuracy of the calibrated displacements. However, the control markers prevent tracking of the soil behind them, and hence must be using sparingly. Figure 3-6 shows the final layout used. As far as possible control markers were kept away from regions where large displacements were expected, or when necessary on lines of symmetry so the missing data could be easily interpolated if required.

Figure 3-6 also shows the GoPRO camera used to capture the stills used in the tracking software. The work by McMahon et al (2013) showed that the deformation mechanism seemed to change most rapidly at low levels of load and settlement. Hence, it was important to record at a high frames per second to allow for accurate tracking of these changes. The trade-off was in ensuring the camera had sufficient memory to capture the full experiment. The camera was placed as close as possible to the Perspex window to aid the tracking software. The limit was the fixed focal length of the camera and needing to capture the soil some distance away from the footing.

Figure 3-7: Vane Shear tests

3.2.7. Vane Shear Tests

In order to quickly determine the undrained shear strength of the clay, vane shear tests were conducted.

The device correlates the resisting torque of the soil to the undrained shear strength. Figure 3-7 illustrates the locations of the tests performed. The top surface was tested as this was the clay mainly resisting the footing movement. Additionally, readings with depth were taken in order to judge the conjecture that constituting from slurry produces uniform, isotropic soil shear strengths. Conducting the tests immediately after the experiments prevented drying out of the clay.

3.2.8. Triaxial Testing

Cylindrical samples were also removed from the clay in order to perform Triaxial testing, with the aim of measuring the undrained shear strength and the soils shear modulus. The cylinders were cored from the top surface downwards, in order to estimate the average properties of the soil the mechanisms sheared.

Unconsolidated-Undrained Triaxial tests (UU-tests) were conducted on 6 samples (2 from each strength experimented on). This meant the rate of loading was sufficiently high that the soil behaved as undrained, in order to reflect the soil conditions in the experiment. Confining pressure was also not applied as the soil beneath the footing would have also felt relatively little lateral stresses during testing. Of course, applying a confining stress would not affect the measured undrained shear strength. The test was conducted following the procedure dictated by the American Society for Testing and Materials (ASTM) standards.

Figure 3-8 illustrates the setup for the Triaxial tests. The confining effect of the membrane was ignored in testing. The ASTM standards describe that for most routine tests the effects will be negligible. Failure was taken to be either the maximum principal stress measured or that measured at 15 % axial strain. This allowed the undrained shear strength to be determined. The loading rate was controlled by an axial strain of 1 % per minute. The shear modulus was inferred from the gradient of half the deviatoric stress against the shear strain.

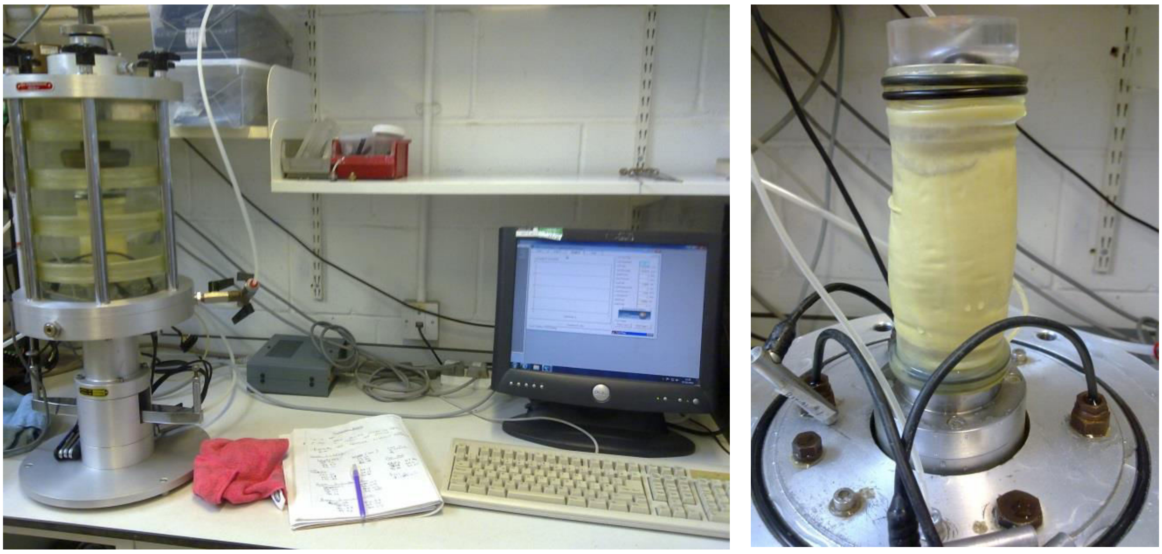

Figure 3-8: Triaxial testing setup, computer controlled test (left) and close up of sample (right)

3.3 Summary of Experimental work carried out

Table 3-1 summaries the experimental work carried out for this project. The test Id defined will be used to identify the experiments in later figures and discussions.

Table 3-1: Summary of experimental work conducted

Test Id	Type of foundation	Nominal Undrained Shear Strength S_u (kPa)	Type of test	Soil Characterisation	
				No. of Vane shear tests	Samples for U-U Triaxial tests
MSC1-a	Strip	25	Plane strain		
MSC1-b	Semi-circular	25	3-D	8	2
MSC1-c	Semi-circular	25	3-D		
MSC2-a	Strip	50	Plane strain		
MSC2-b	Semi-circular	50	3-D	16	2
MSC2-c	Semi-circular	50	3-D		
MSC3-a	Strip	100	Plane strain		
MSC3-b	Strip	100	Plane Strain	16	2
MSC3-c	Semi-circular	100	3-D		

4. Experimental Results

This section presents a selection of the experimental results obtained. A more complete discussion of the experimental results will follow in Section 5.

4.1 Visualising Deformation Mechanisms

The first consideration for visualising the deformation mechanism is to gather evidence of the 'changing deformation mechanisms' observed by McMahon et al (2013a).

Figure 4-1 shows the 'smoothed PIV results' from the strip footing on soil of a nominal undrained shear strength of 25 kPa. The smoothing of the displacement fields was achieved by taking a weighted average of neighbouring values.

We are interested in the changing mechanism beneath the footing. The results show the displacement vectors over intervals of 10 seconds. The 1D actuator moved with a constant velocity hence the 'time since start' can also be thought of as an indication of the settlement of the footing. A magnification of × 10 is used on the actual soil movements.

Observing Figure 4-1 clearly indicates the deformation mechanism beneath the strip footing is changing with time, or more specifically with displacement of the footing. Utilising the fact that the actuator drove the footing at 0.1 mm s^{-1}, it can be roughly estimated that by a displacement of between 6.5 and 8.5 mm the 'ULS' deformation mechanism, or final failure mechanism is reached. By this we mean the shape of deformation mechanism no longer changes and the footing is in limiting equilibrium with the applied load. At this ULS load the movement of the soil is very similar to that predicted by the Prandtl Upper bound solution. Three rigid triangles can be observed, the central moving vertically down and the left and right moving diagonally upwards at 45°. Between these regions the two slip fans can also be discerned, featuring many infinitesimal rigid elements moving along an arc. The limit of the assumption of rigid-perfectly plastic soil can be witnessed in the figure, as soils outside the theoretical regions are also moving. The mechanism is hence sometimes described as a Prandtl+ mechanism.

As the settlement increases, we observe the 'extent' of the deformation mechanism appears to change. At low settlements a large volume of soil mass moves in small amounts to accommodate the footing displacement. There is little discernable upwards movements or 'heaving' of the soil. As the footing displacement increases however the soil adjacent to the footing begins to heave, eventually leading to the Prandtl+ Mechanism. In such mechanisms a smaller volume of soil displaces a larger amount to accommodate the footing settlement.

Figure 4-1: Smoothed PIV results, deformation mechanisms from test MSC1-a

Time since start (s)	Smoothed PIV results
5 -15	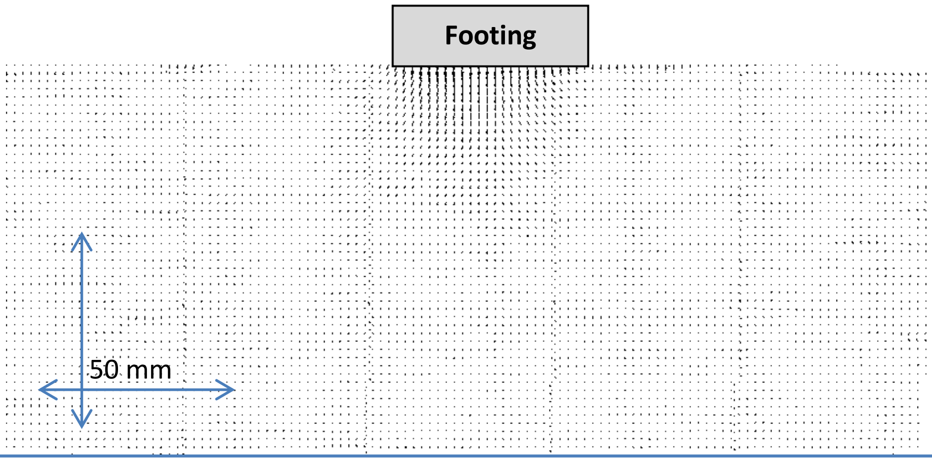
20 - 30	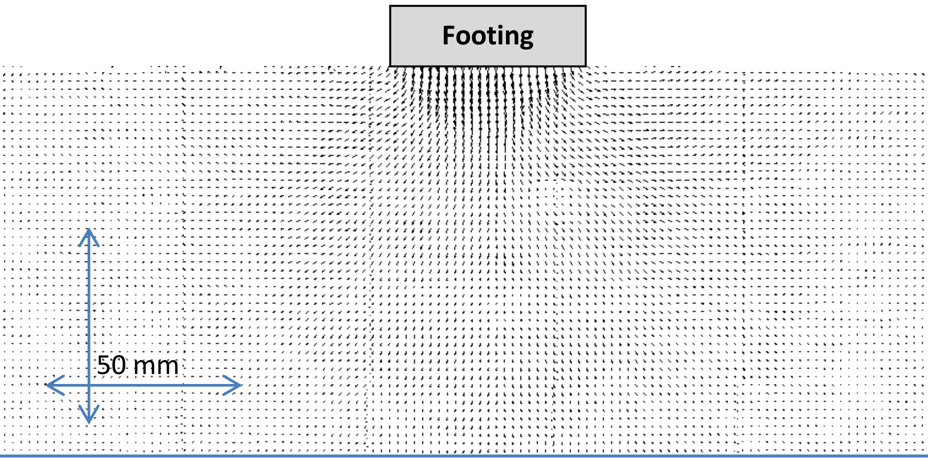

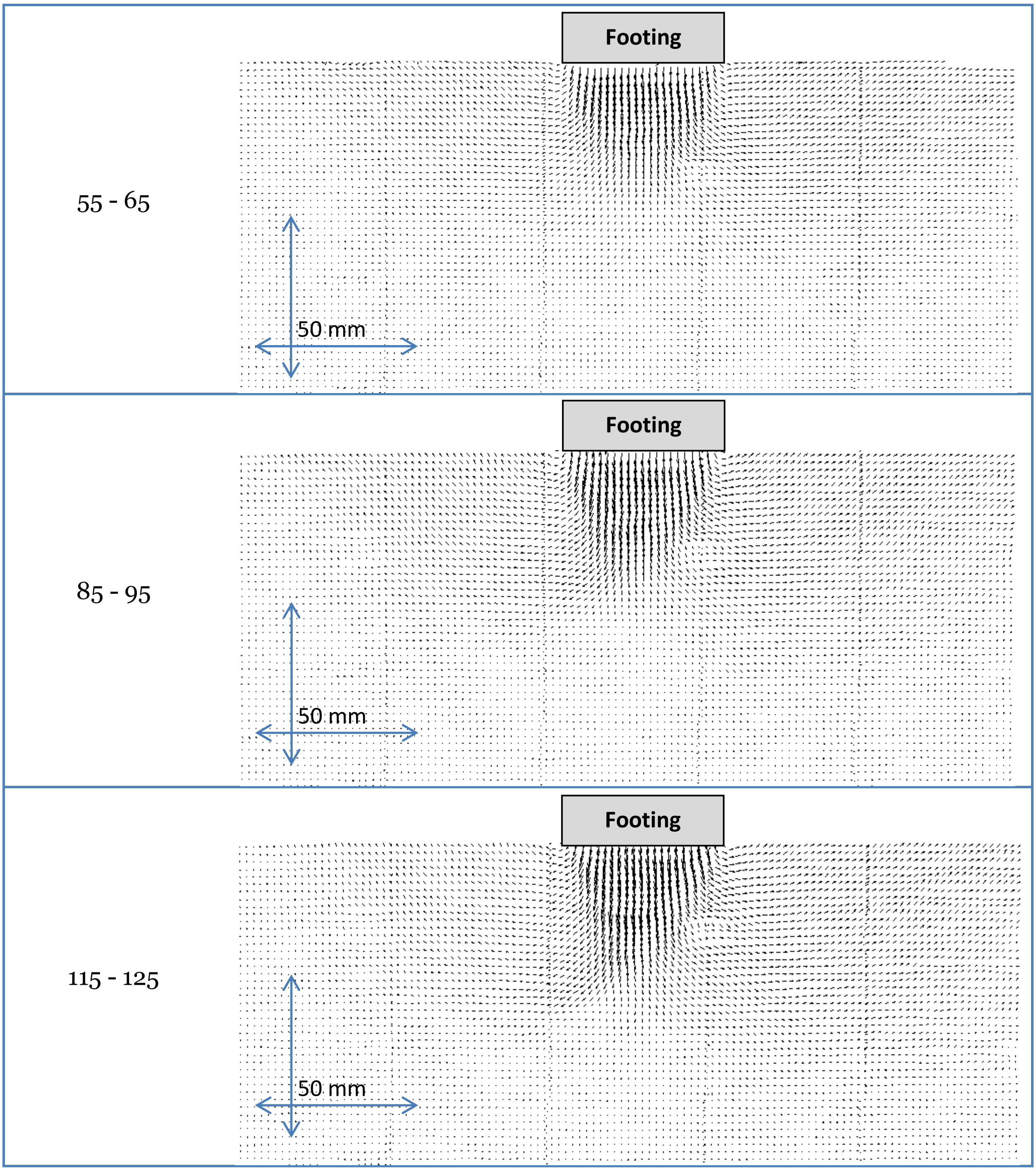

Figure 4-2 shows the smoothed PIV results for the changing deformation mechanism with time beneath a circular footing. Time intervals are again 10 seconds (corresponding to a footing displacement of 1 mm) and a magnification of × 10 on the soil displacements is also used once again.

Figure 4-2: Smoothed PIV results, deformation mechanisms from test MSC1-b

Time since start (s)	Smoothed PIV results
5 -15	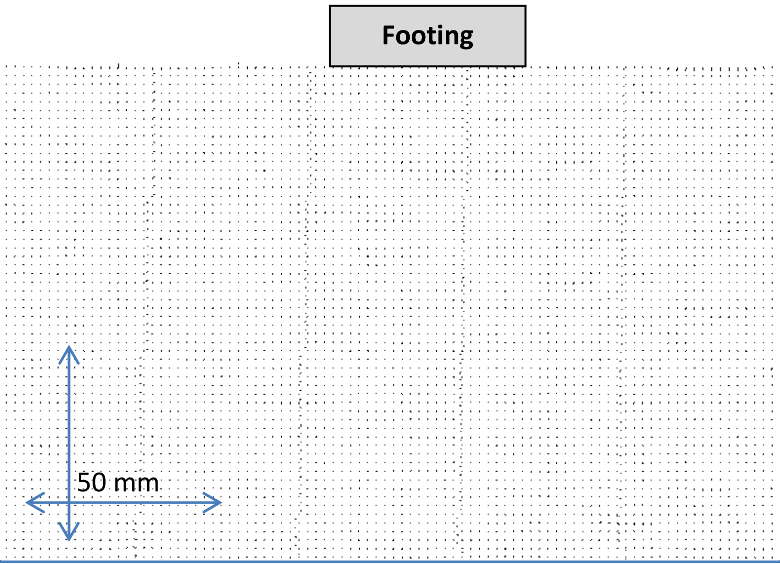
20 – 30	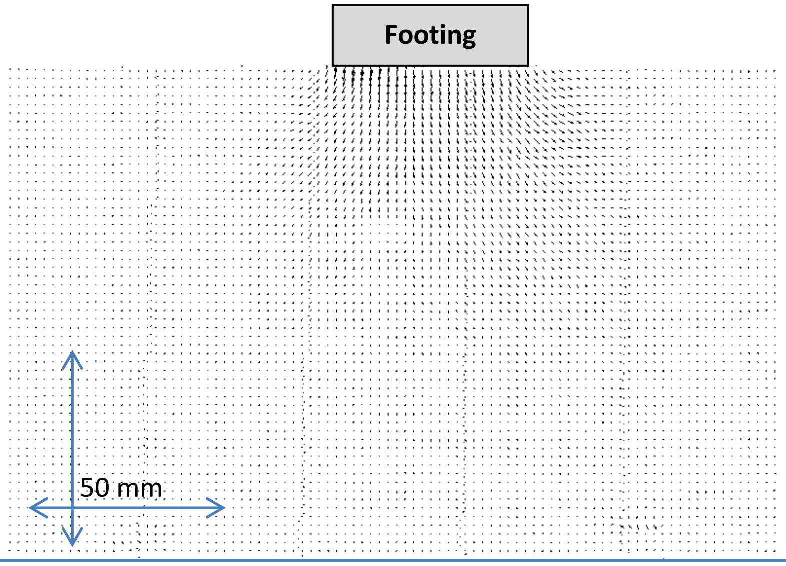
55 – 65	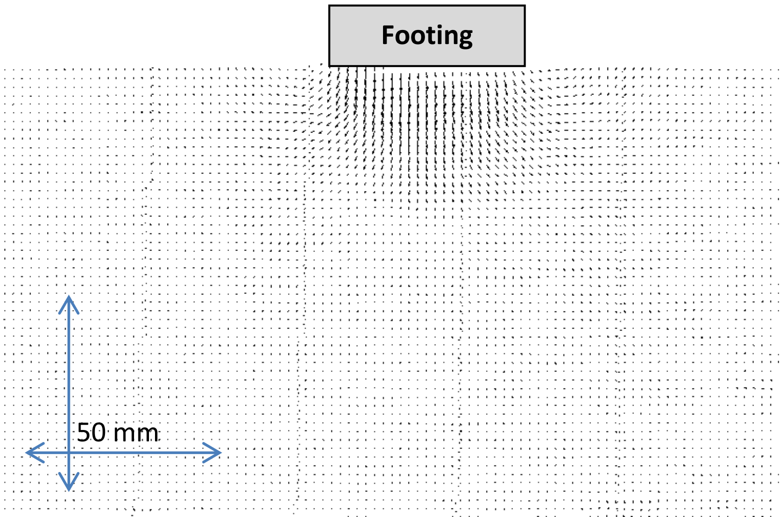

85 – 95	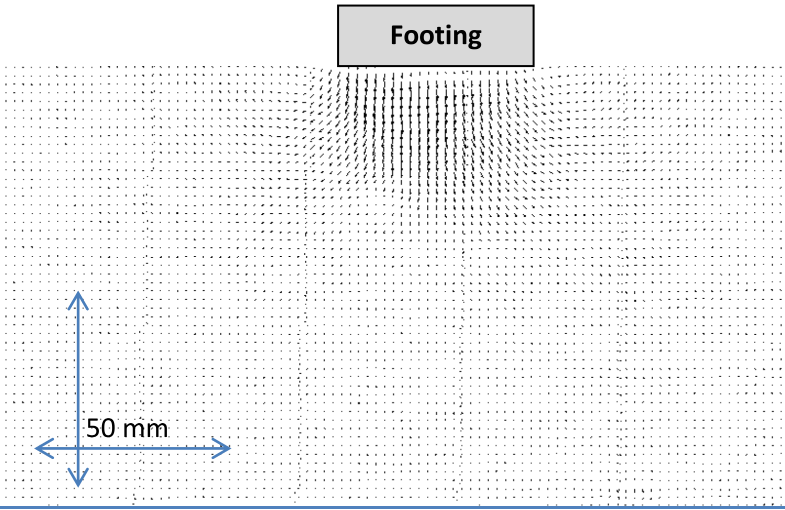
115 - 125	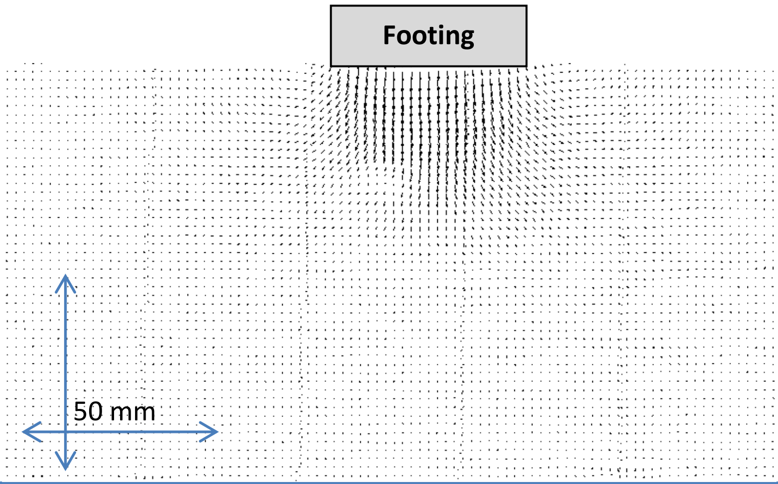

A similar trend of changing deformation mechanisms to that observed previously in Figure 4-1 for the strip footing can be discerned for the circular footing as well. However, the main difference is that the 'ULS' deformation mechanism (again resembling a 'Prandtl+' mechanism) appears to be reached at much smaller displacements of the footing. The other main difference is the magnitude of the soil movements is smaller. This is easily rationalised by appreciating the circular footing displacement can be accommodated by the soil moving outwards in 3 dimensions, which in turn implies smaller movements of each soil particle.

Figure 4-3 shows the recorded deformation mechanism at the time t = 85 – 95 s from three strip footing and three circular footing tests on soils of nominal undrained shear strength 25, 50 and 100 kPa. Again, a magnification of × 10 and smoothing function is used on the soil movement.

Figure 4-3: Smoothed PIV Results, deformation mechanisms from various tests at time t = 85 – 95 s

Test ID	Smoothed PIV results Strip Footing	Circular Footing
MSC1	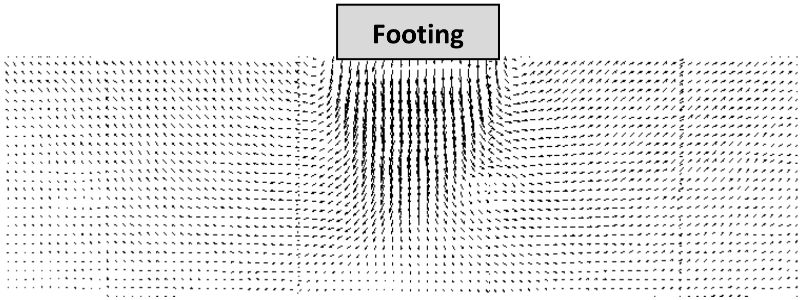	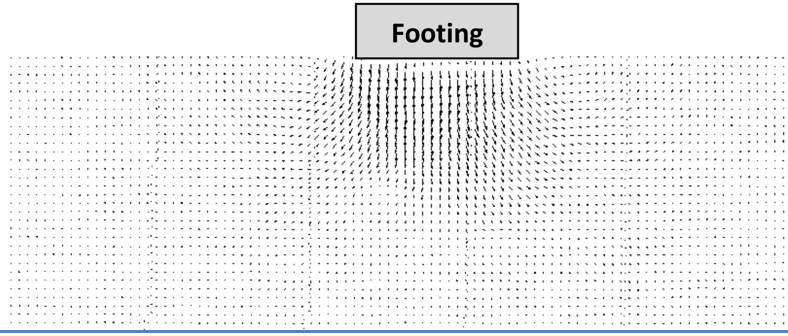
MSC2	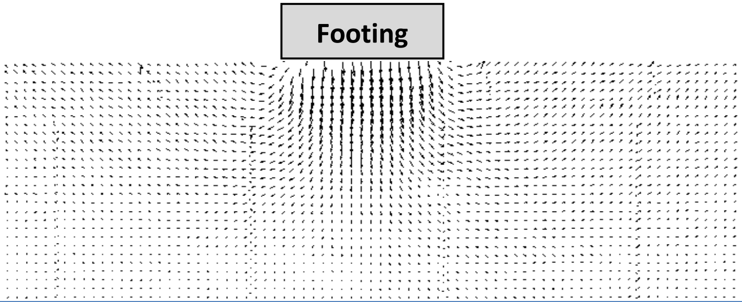	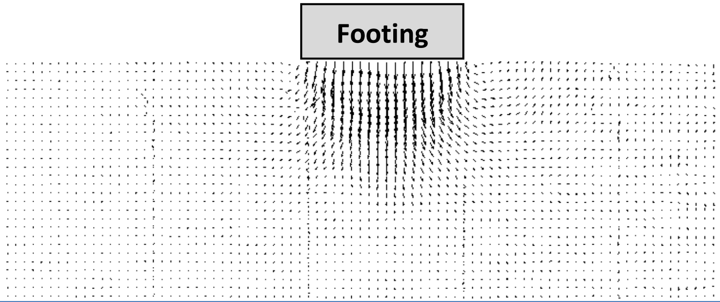
MSC3	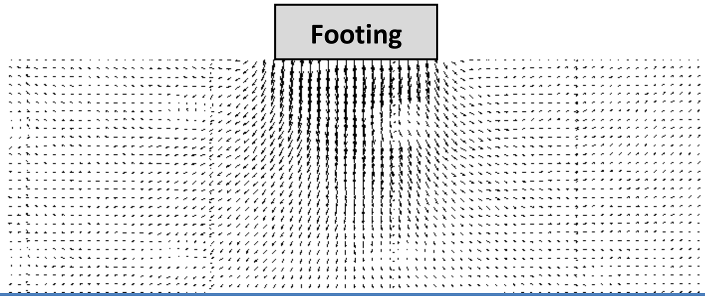	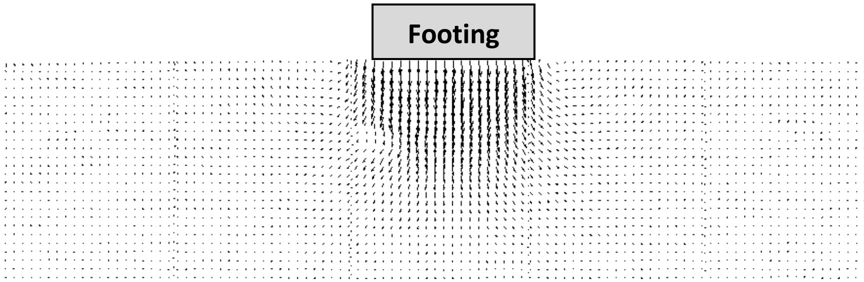

Figure 4-3 illustrates that the observed deformation mechanisms are not only restricted to the soft clay results presented in Figure 4-1 and Figure 4-2, but were reproduced in the tests on stronger and stiffer clays. Based on Figure 4-3 it can be seen that at the same time, and hence footing displacement the deformation mechanisms all appear very similar in terms of type. It can be tentatively suggested at this stage that the changing deformation mechanism may be independent of the soil properties. The reason the magnitudes of the soil movements appear similar despite the soil in the tests having different strengths and stiffness' is that the GeoPIV plots shown are taken from the same footing displacement, not the same applied load. Indeed, the fact the magnitudes of the soil displacements appear so similar does suggest that load-settlement behavior can be normalised to be made independent of the soil properties.

The influence of the soil properties on 'when' (in terms of settlement) the mechanism switches will be further explored in Section 5.2.

4.2 Load-Settlement Measurements

By combining the recorded measurements from the load cells and LVDT the measured load-settlement behaviour for the footings can be obtained. Figure 4-4 shows these results for the strip footing on the three nominal undrained shear strengths. Similarly, the measured load-settlement plots have been obtained from the five tests on circular footings, and are presented in Figure 4-5. In both Figures, the data presented has been filtered as described in Section 3.2.4 and a smoothing function used. The smoothing function used a moving average of the recorded data points to produce the plotted line. Both measures were taken to remove the noise in the signal, whilst attempting to minimise distortion to the gradient or average of the recorded values.

Both figures also feature the implied undrained shear strength from the load plateau, based on the Eurocode ULS predictions (i.e. accounting for the shape factor). These will be compared to more direct measurements in Section 4.3 and Section 4.4.

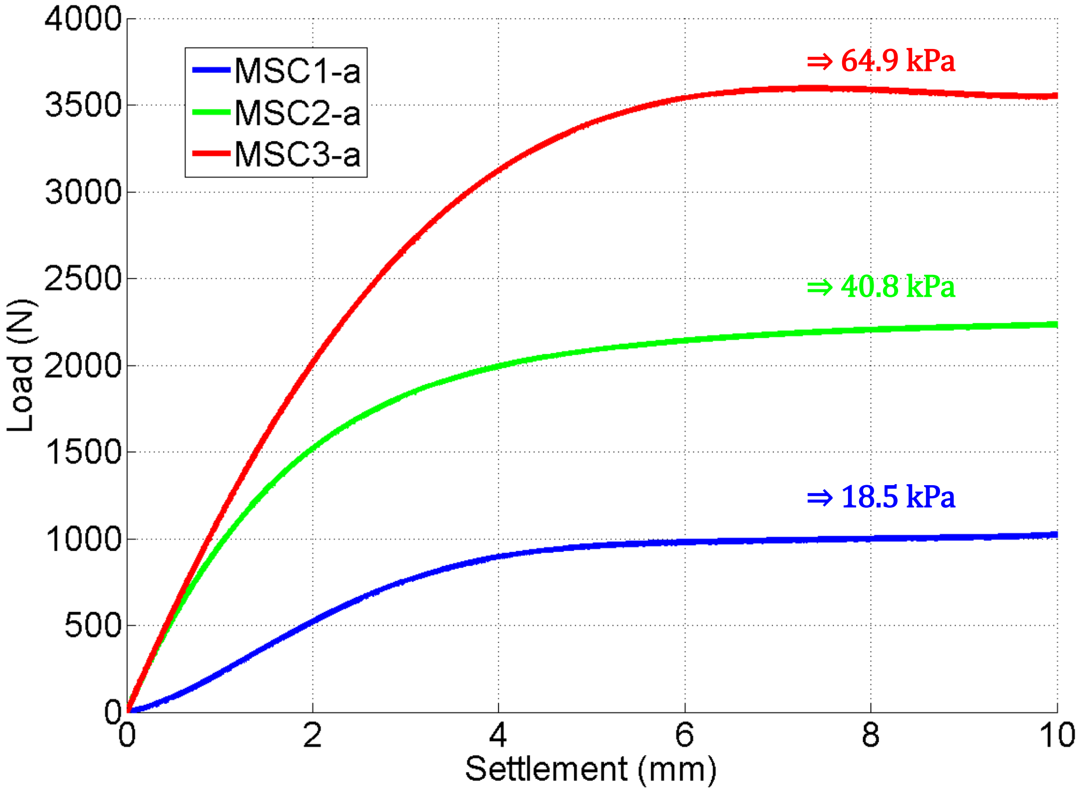

Figure 4-4: Measured Load Displacement behaviour for Strip footings

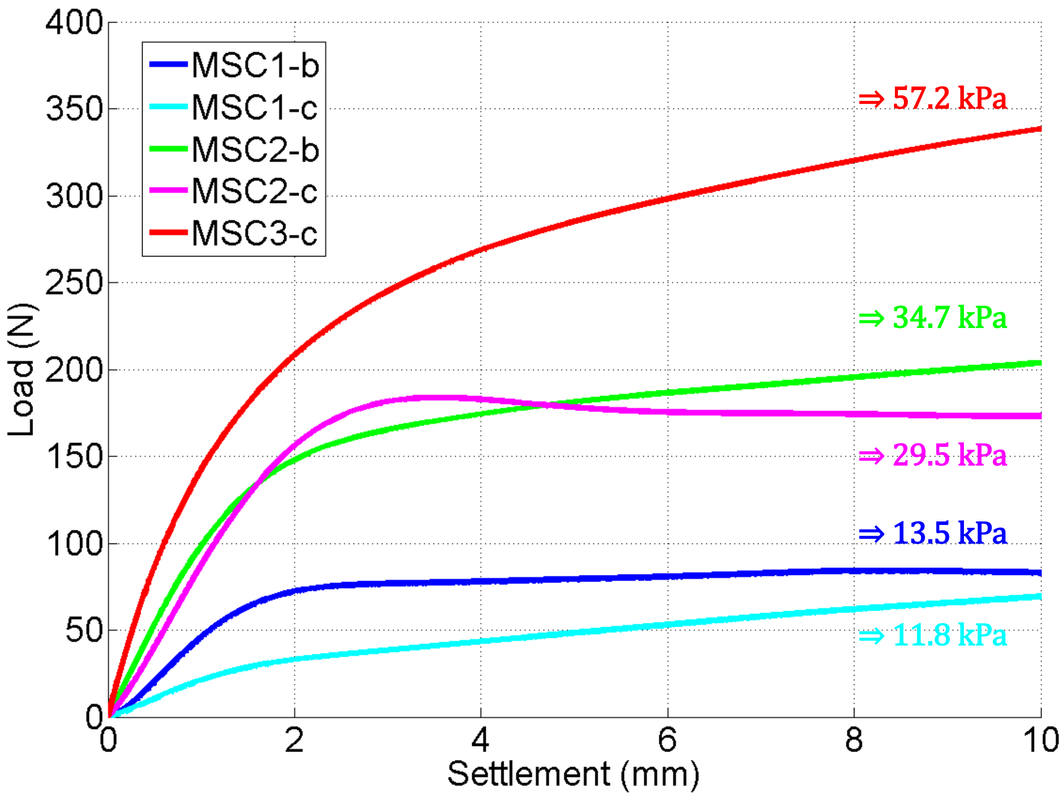

Figure 4-5: Measured Load Displacement behaviour for Circular footings

4.3 Vane Shear Test results

Section 3.2.7 describes the vane shear tests carried out in order to quickly ascertain the undrained shear strength of the clays consolidated from slurry. The results are presented in Table 4-1, alongside a summary of the values implied by the load-settlement curves. The approximate locations of the vane shear tests are illustrated by Figure 3-7.

Table 4-1: Results from Vane Shear tests and load-settlement curves

	Test Id	MSC1	MSC2	MSC3
Vane Shear tests	Top Surface Average (kPa)	24.29	40.17	62.00
	Standard Deviation (kPa)	3.05	1.21	3.06
	Depth Average (kPa)	Not Measured	30.70	46.07
	Standard Deviation (kPa)	N/A	0.78	6.79
Implied by load-settlement curves	Strip Footing (kPa)	18.50	40.80	64.90
	Circular Footing average (kPa)	12.65	32.1	57.2

From Table 4-1, a good agreement between the strip footing results and the vane shear tests can be observed. This is largely the case for the circular footing as well, although the matches are less close for softer soils. It is possible this is due to two reasons.

As discussed in Section 3.2.3, the miniature diaphragm load cells used were very sensitive to moment loads, and hence a small rotation of the footing could have affected the calibration values. The second possible reason is the circular footings had a considerably smaller plan area than the strip footings, and therefore act over a smaller surface of clay. The measurements are hence more sensitive to any anisotropy in the clay properties along the surface. The clay nearest the edges is more likely to swell and soften when the front plate was replaced with a Perspex window – hence potentially explaining the lower values recorded by the circular footing.

4.4 Triaxial Testing Results

The Triaxial tests were conducted following the procedure laid out in Section 3.2.8. Figure 4-4 illustrates the results from the second batch of samples. The deviatoric stress against axial strain percentage and half the deviatoric stress against the non-dimensional shear are plotted. These facilitate the calculation of the undrained shear strength and shear modulus respectively, as summarised in Table 4-2. The piston used in the Triaxial testing apparatus became stuck at low loads during the first set of testing, and this resulted in the initial part of the stress strain response not being recorded. Therefore, in Table 4-2 the shear modulus is calculated based on only the second batch of experiments. The undrained shear strength could nevertheless be inferred from all batches of clay tested.

The agreement between the average values from the Triaxial tests and the vane shear tests from the top surface increases our confidence in these values. The average values were used in order to mitigate for the uncertainty present in both tests. It is possible the first test under estimated the peak values due to the piston 'jumping' after having become stuck. Conversely, the second test may have overestimated the peak value as it was conducted a few weeks after the first test, in which time the clay may have age hardened.

Nevertheless, although the shear modulus could only be obtained from the Triaxial tests, the overall ratio of the shear modulus to undrained shear strength agrees satisfactorily with the predictions from the relationships suggested by Houlsby and Wroth (1991).

Table 4-2: Summary of results from Triaxial tests

Test Id	**Max Observed S_u (kPa)**			**Shear Modulus G (MPa)**	$\frac{G}{S_u}$
	Sample 1	Sample 2	Average	Test 2	
MSC1	31.19	23.25	27.22	0.084	3.09
MSC2	35.74	82.43	59.09	0.488	8.26
MSC3	41.13	144.37	92.75	1.104	11.90

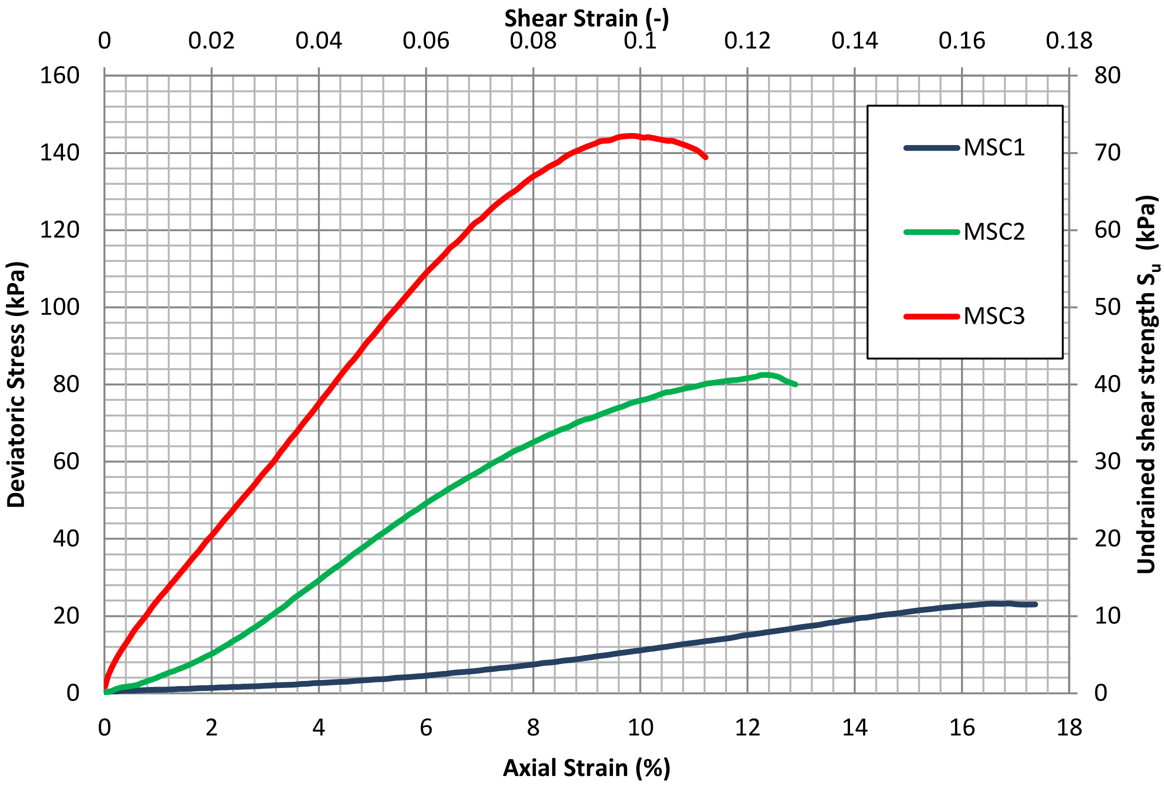

Figure 4-4: Results from Triaxial tests, plotted to allow determination of undrained shear strength and the shear modulus

5. Discussion and Further Analysis

5.1. Visualising the changing deformation mechanism

From Figure 4-1 and Figure 4-2 it can be concluded that for both footings, prior to the ULS settlement there is significant deviation from the predicted Prandtl mechanism. The previous centrifuge experiments by McMahon et al (2013a) on circular footings also produced similar results to those observed in Figure 4-1. In this work the deformation mechanism was described using a cavity expansion model, and it was demonstrated that such a model agrees well with previous numerical analyses. Qualitatively, our deformation fields and those obtained by McMahon et al (2013a) are similar.

Whilst this alone does not necessarily validate the cavity expansion model proposed by McMahon et al (2013a), we can already draw one very important conclusion. All experimental data to date certainly suggests that using a Prandtl deformation field to model the displacements of the soil at small settlements of the footing is inaccurate. In terms of design, if one were to use the Prandtl mechanism to calculate the displacements of a footing given a certain applied load, the result would be erroneous. Further, if the actual deformation mechanism that occurs implies a larger settlement at the same load, it is quite possible that either the SLS or ULS of the supported superstructure may be breached. This key design idea will be explored further in Section 5.2.

In order to better visualise the movements of the soil, a Matlab Script, originally written by Hanselman (2008) and edited by the author, was used to find the 'streamlines' of the soil movements using the GeoPIV data. This script essentially calculates and plots the 'steepest gradient' of the inputted matrix of data. Combining these with the load-settlement plots leads to very clear illustrations of the changing deformation mechanism as the footing settles. Observing Figure 5-2 and Figure 5-3 in conjunction allows for some interesting conclusions to be made. The extent of the strip footing mechanism, as explained in Section 4.1, is larger than the circular footing, as evident from the streamline plots from the lowest settlement.

The mechanisms for both footings seem to change in a similar fashion. Soil movements are initially mainly vertical. As the load is increased regions near the edges of the footing tend to accumulate horizontal as well as vertical displacements. As the load is further increased, the soil in these regions displaces sideways and upwards – towards the free surface.

Though this pattern of change is similar for both mechanisms, it is considerably more rapid for the circular footing. We may conclude that a circular footing will be able to reach the ULS settlement with much less settlement than a strip footing with a width equal to the circular footings diameter. In terms of design, we must hence be more cautious when using the ULS load predicted by the Prandtl mechanism for a strip footing –as it would have undergone considerable settlement by this level of loading. Indeed, codes of practice do use larger factors of safety for the SLS calculations for strip footings than circular footings.

Having established that the deformation mechanism is changing, we must next attempt to explain why such a phenomenon occurs. From an upper bound viewpoint, we can argue that the soil displaces in such a manner as to minimise the energy dissipated in the soil mass. The energy dissipated in the soil is due to relative shearing between the soil particles. We assume the loading is sufficiently fast that the pore water cannot leave the pore space, and hence the soil movements are constrained by the fact no volume change can occur. In the case of large displacements, it is hence expected that the soil around the footing will 'heave' upwards to allow this zero volume change condition to be satisfied. The circular footing permits this 'heaving' in three dimensions, and hence the overall movements will of course be smaller. The GeoPIV results confirm this behaviour, the soil does indeed move towards the 'free surface' at large footing displacements.

In theoretically perfect undrained conditions, no deformation mechanism exists with only vertically downwards soil movements. The zero volume change condition can simply not be satisfied without some 'heaving' of the soil near the surface. Of course, in our experiment, and indeed in reality, such conditions are not maintained. The 'free surface' of the soil will of course permit near instantaneous consolidation, having a drainage distance of essentially zero. It can hence be theorised that at very small loads and induced settlements, the soil is able to accommodate the footing displacement without 'heaving' near the surface. As the footing displacement increases, deeper soil will also permit some pore water to leave allowing small amounts of volume change. The accumulation of these small volume changes as the soil mass densifies essentially describes the 'elastic' deformation mechanisms observed. Eventually however the footing displacement becomes too large to be accommodated in this manner and there is less energy dissipated by formation of a Prandtl like mechanism, leading to the deformations seen along the plateau of load-settlement curve.

In order to investigate this theory that the undrained conditions may not be perfectly maintained, the distribution of volume changes across the soil mass were inferred from the recorded GeoPIV measurements. The volume change was calculated from appropriately summing the soil strains calculated for the upper bound calculations, which will be discussed in more detail in Section 5.3. Figure 5-1 illustrates the distribution of volumetric strains beneath the strip footing, based on the GeoPIV data from the lowest settlement shown in Figure 5-2. The distribution of volumetric strains does indeed suggest that small footing displacements can be accommodated by densification of the soil mass as small amounts of pore water leave the pore space.

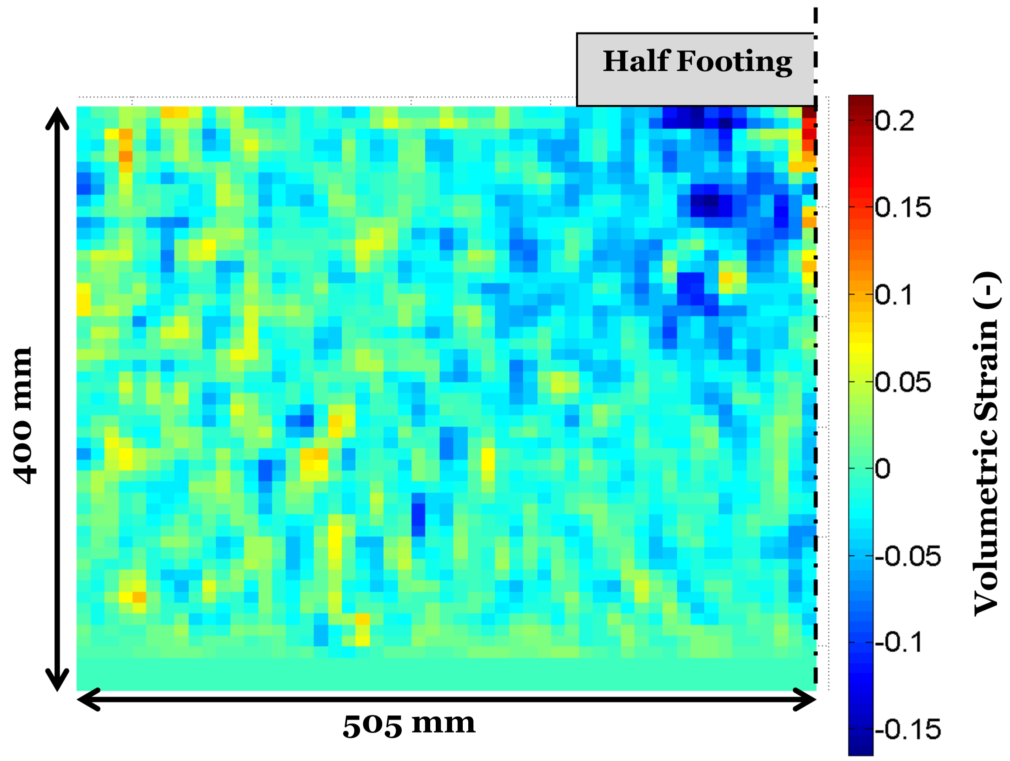

Figure 5-1: Plot of Volumetric strain beneath strip footing, inferred from GeoPIV data

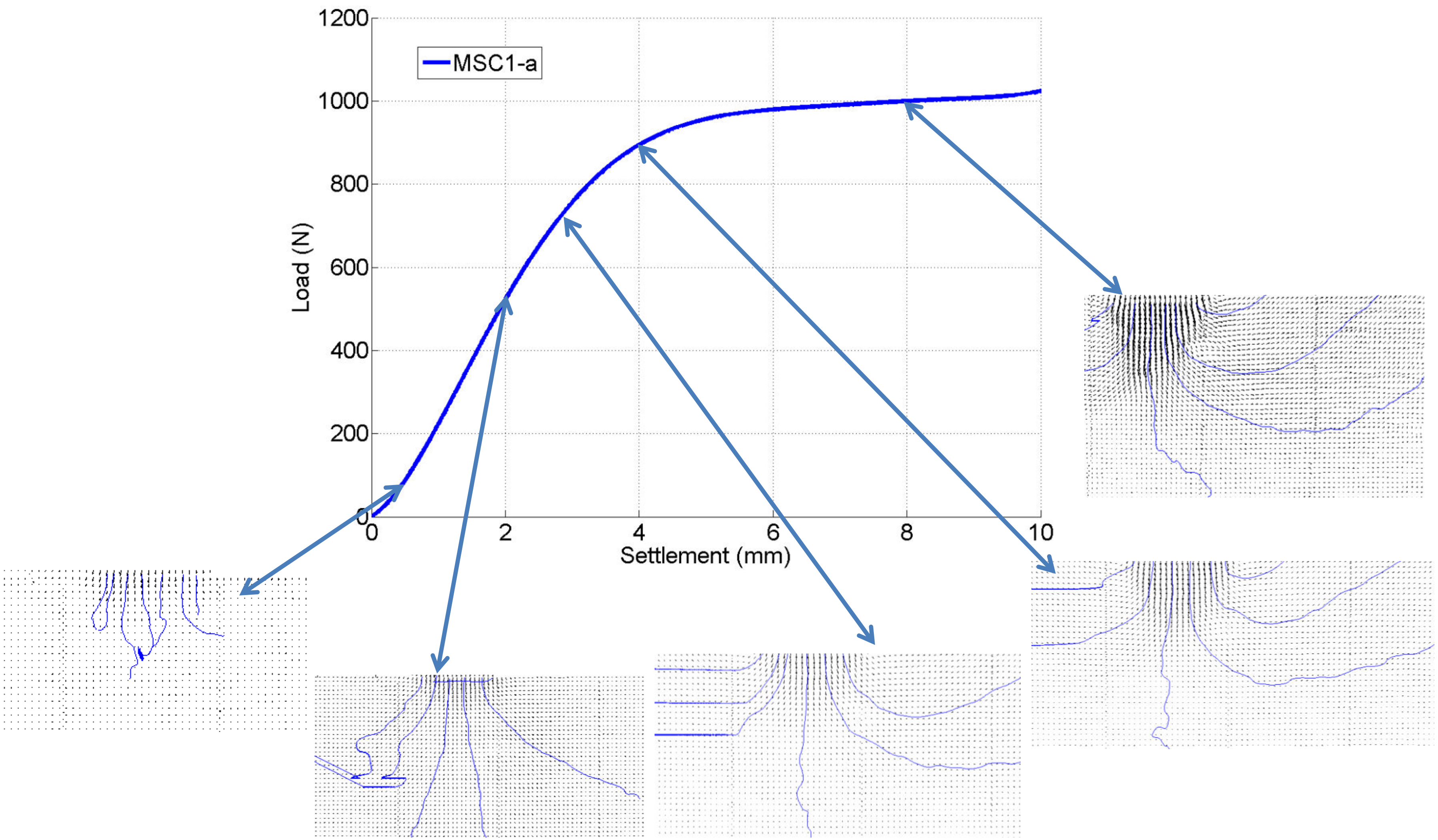

Figure 5-2: Visualising soil movements and combining with load settlement measurements for test MSC1-a

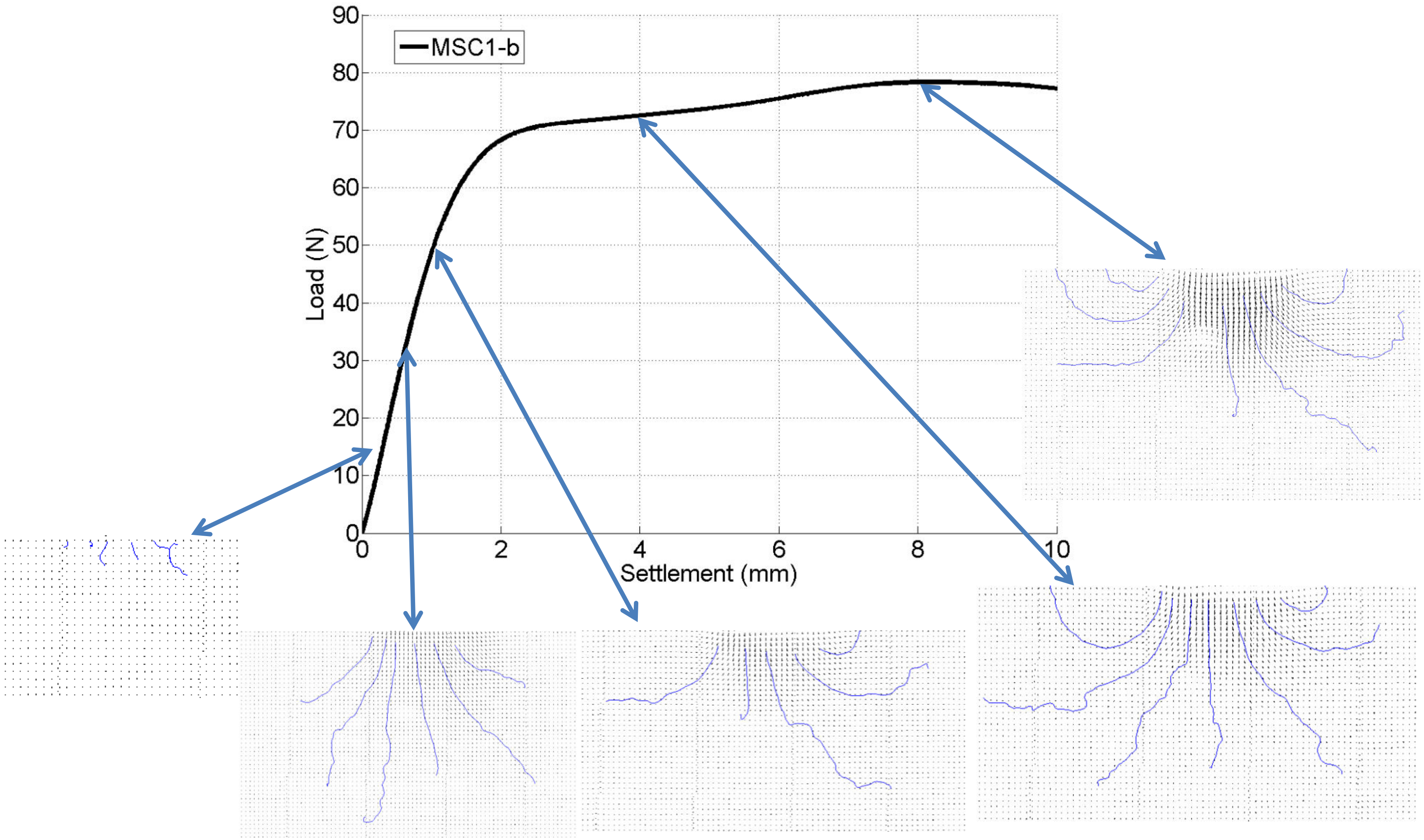

Figure 5-3: Visualising soil movements and combining with load settlement measurements for test MSC1-b

5.2. Normalising the Load-Settlement Behaviour

McMahon et al (2013a) normalised the load settlement behaviour by considering instead the bearing capacity factor (the footing pressure divided by the undrained shear strength) against the non-dimensionalised settlement (the ratio of the footing displacement to the footing diameter multiplied with the ratio of the shear modulus to the undrained shear strength).

In order to normalise our experimental results in a similar fashion, the undrained shear strength and shear modulus were required. Rapid estimates of the undrained shear strength were obtained from the vane shear test, the results given in Section 4.3. The results from the Triaxial testing, Section 4.4, also gave an indication of the undrained shear strength. The potential for error and the relative accuracy of these tests has been discussed in Section 5.2. The average values and ratios given in Table 4-1and Table 4-2 respectively will be used to normalise the experimental data.

In theory, all sets of experimental results should then collapse into one single line – we predict that the change of deformation mechanism and normalised load settlement behaviour is independent of the soil properties. Further, this line should define the lower envelope of results predicted by McMahon et al (2013b).

In this work, the 'optimal displacement mechanism' beneath circular shallow foundations was investigated from a theoretical viewpoint. A non-linear constitutive relationship was used to accurately model the soil behaviour, using the parameters defined by Vardanega et al (2012). Essentially, upper bound estimates of the load required to induce certain displacements of the footing were calculated for a range of deformation mechanisms. The work done was simply the load on the footing multiplied with the displacement. The energy dissipated in the soil was calculated following the method described by McMahon et al (2013a). Strains in the soil were calculated using the formulation presented by Osman and Bolton (2005), given in equation 5.1a. The plastic and elastic energy dissipated can be calculated based on equation 5.1b, though a numerical integration scheme was employed in practice.

$$d\varepsilon = \frac{1}{2}\left[\nabla d\bar{u}(\chi) + \left(\nabla d\bar{u}(\chi)\right)^{\mathrm{T}}\right] \qquad \textbf{Equation 5-1a}$$

$$\mathrm{d}E = \int_V \sigma_{ij}\mathrm{d}\varepsilon_{ij}\mathrm{d}V = \int_V 2c_\mathrm{m}[\varepsilon_\mathrm{s}]\mathrm{d}\varepsilon_{\max}\mathrm{d}V \quad \textbf{Equation 5-1b}$$

where, dε-strain increment, du-displacement increment, χ-coordinate, dE-internal work increment, σ-stress tensor, dV-volume increment, c_m*-mobilized strength, ε- strain tensor*

By running this script for various deformation mechanisms, McMahon et al (2013b) could test for the change of mechanism experimentally observed by seeing whether different mechanisms became optimal (required less load for a given settlement) at different points in the load settlement space. The results from using a 'linear-elastic perfectly plastic' constitutive soil model and the Von Mises stress criterion for soil failure is presented in Figure 5-4, alongside previous results from literature.

As well as the good agreement between the theoretical predictions and previous numerical analyses, the work also reveals some interesting predictions. At very small settlements of the footing, the elastic deformation mechanism (generated from a linear elastic finite element analyses in ABAQUS) produces the lowest upper bound prediction. It is observed however that at the typical footing 'working loads', the cavity expansion model described by McMahon et al (2013) is more optimal. The final switch comes at much larger settlements, at which point the Prandtl mechanism (or specifically a field described by Osman and Bolton (2005) that uses the 'outline' of the Prandtl mechanism but includes distributed plastic strains) becomes optimal.

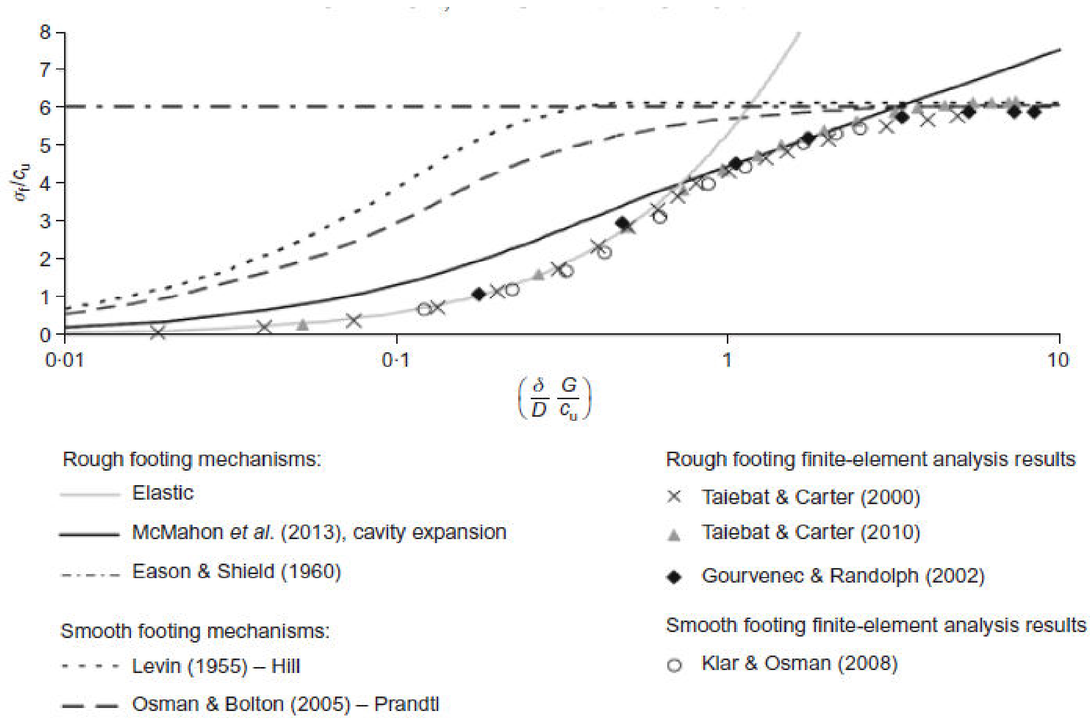

Figure 5-4: Optimal displacement mechanism beneath circular footings, following McMahon et al (2013a)

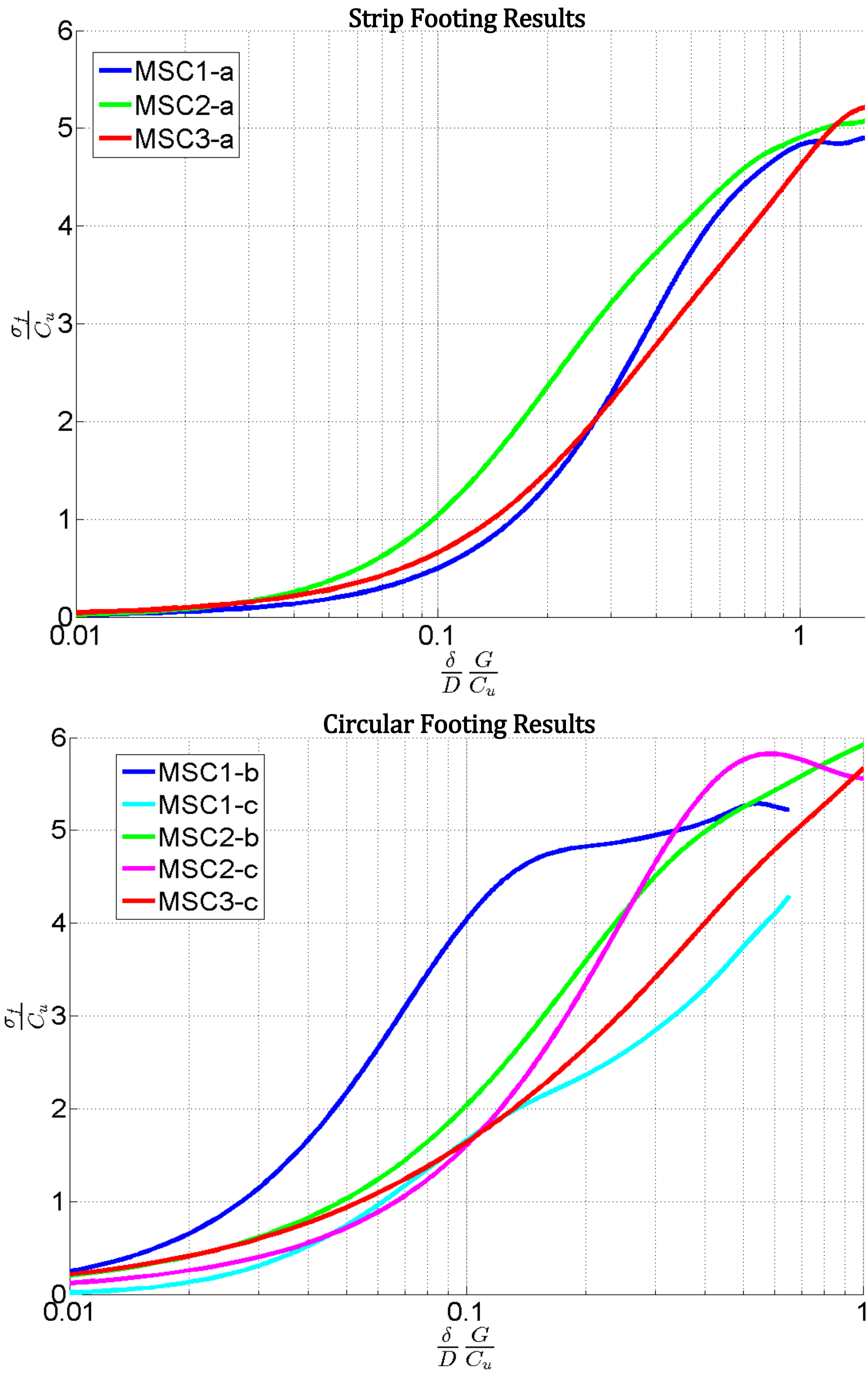

Figure 5-5: Normalising experimentally determined load settlement behaviour following from McMahon et al (2013a)

Figure 5-5 evidences that the load settlement behaviour can indeed be normalised to be made independent of the soil properties. Uncertainty in the determination of the soil parameters, and potentially in the calibration of the load cells or LVDT can explain the slight discrepancies between the curves. This has been previously elaborated upon in Sections 4.2 and 4.4. Nevertheless, these differences are well within the expected experimental tolerances.

5.3. Upper Bound Analyses

The beauty of the Upper Bound method is that any compatible deformation mechanism can be constructed, the energy dissipated evaluated and the load-displacement behaviour for that mechanism inferred. Figure 5-4 illustrates how this procedure was previously carried out for various deformation mechanisms, using the MATLAB script first presented in McMahon et al (2013a) to calculate the energy dissipated beneath the circular footings. In order to use these ideas for this experiment, the MATLAB script was modified by the author for use with plane strain systems. To validate these modifications, the rigid block movements predicted by the Prandtl upper bound were inserted into the modified energy script. The following Sections will consider various different methods of predicting the load-settlement behaviour, before concluding with a comparison of the methods attempted.

5.3.1. Validating the energy script

Figure 5-6 shows the results from these calculations. Half of the inserted deformation mechanism is shown and the associated plastic and elastic work (per unit area) at the final load is illustrated. As expected, there is zero elastic work at the ULS load. The plastic work also broadly shows the expected results; there is a constant value of energy dissipated along the two planes at 45°, and around and in the stress fan. The fluctuation of the stress fan boundary values is due to the use of a square mesh of points to define a circular arc. The energy dissipated in the stress fan is equal to the energy dissipated along the stress fan boundary, but appears smaller as it is spread across the stress fan area. The plot of normalised load against settlement gives a final normalised bearing capacity of 5.20. This is approximately equal to the expected theoretical value of 5.14, and hence we may have confidence in using the modified energy script for further comparisons. The normalised horizontal axis used an average value of G/Su.

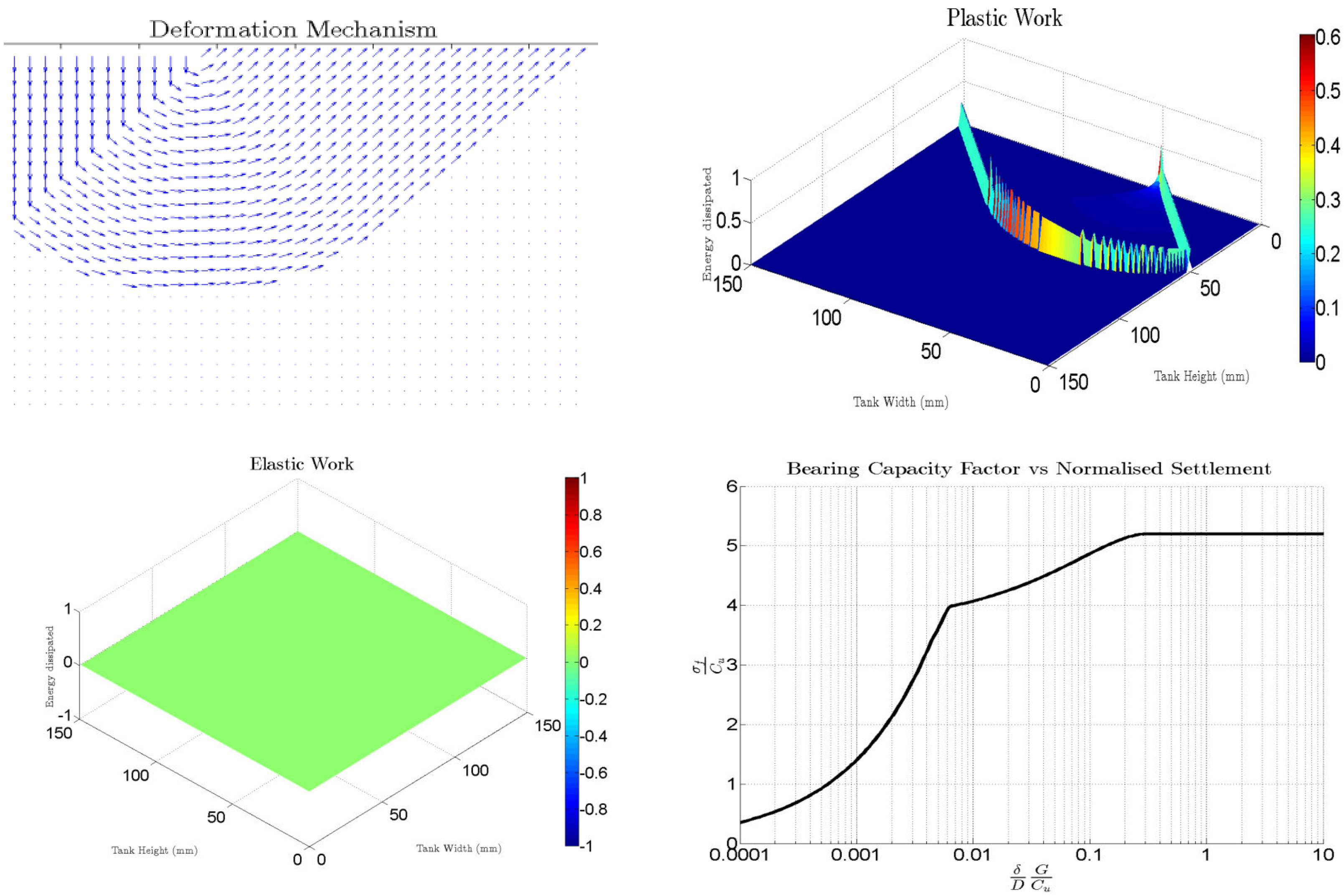

Figure 5-6: Validating energy calculations for plane strain soil conditions

5.3.2. Upper bound analyses for idealised fields

It was discussed in Section 5.1 how the deformation mechanism appears to transition from an 'elastic' mechanism at very small settlements to a field resembling that predicted by Prandtl at larger settlements. Hence, one method of predicting optimal deformation fields may be to combine these fields in various proportions in order to find the lowest upper bound load at any given settlement. This concept is introduced and rationalised by Klar and Osman (2008).

This method is illustrated in Figure 5-7 for circular foundations. The deformation field from an elastic analysis using ABAQUS is linearly mixed with the deformation field following from Osman and Bolton (2005), hereafter referred to as the 'Osman field'. The mathematical description of the Osman field can be found in Appendix A.

It is clearly illustrated that the fields with the higher proportion of the 'ULS mechanism' or Osman field become optimal at larger displacements. Even with this fairly discretised mixing we can observe three transition points between the different mixes of fields. These are highlighted by the red circles shown in the figure.

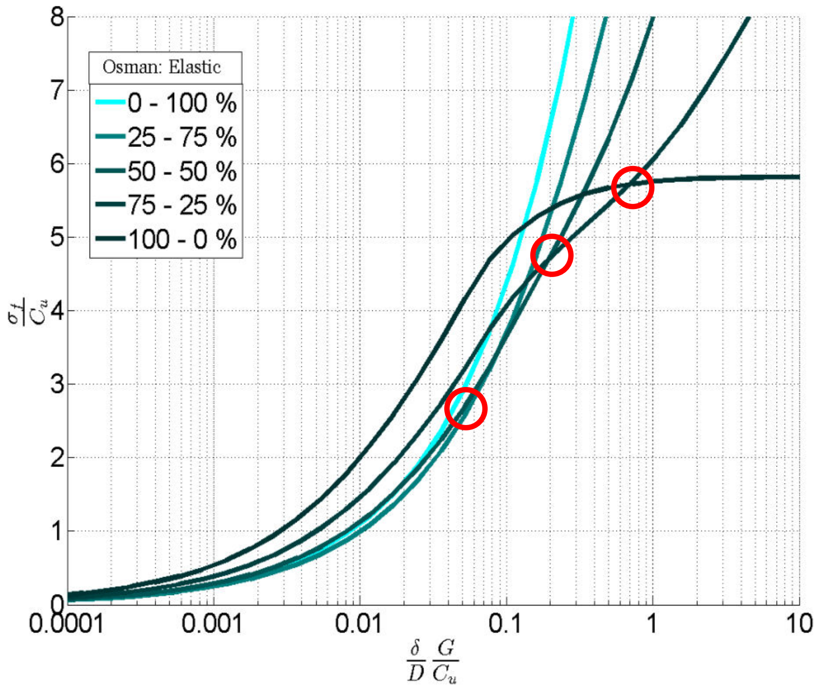

Figure 5-7: Illustration of mixing idealised fields to produce optimal mechanisms

Figure 5-8 illustrates performing the same analyses for continuously varying proportions of the Osman field, but for clarity only 5 % increments are plotted. Figure 5-9 indicates the proportion of the Osman field to the elastic field that produces the lowest required load for each normalised settlement. It is very interesting to note that the lower plot exhibits two plateau's. Previous experimental work has suggested that a Prandtl like mechanism occurs at the ULS load, explaining the near 100 % proportion of Osman field at large levels of footing displacement. However, the fact that a mix of approximately 22 % of the Osman field with the elastic field produces a more optimal deformation mechanism than the pure elastic field is a relatively novel finding. McMahon et al (2013a) described the pure linear-elastic mechanism as being optimal in similar regions, before transitioning into a cavity expansion mechanism.

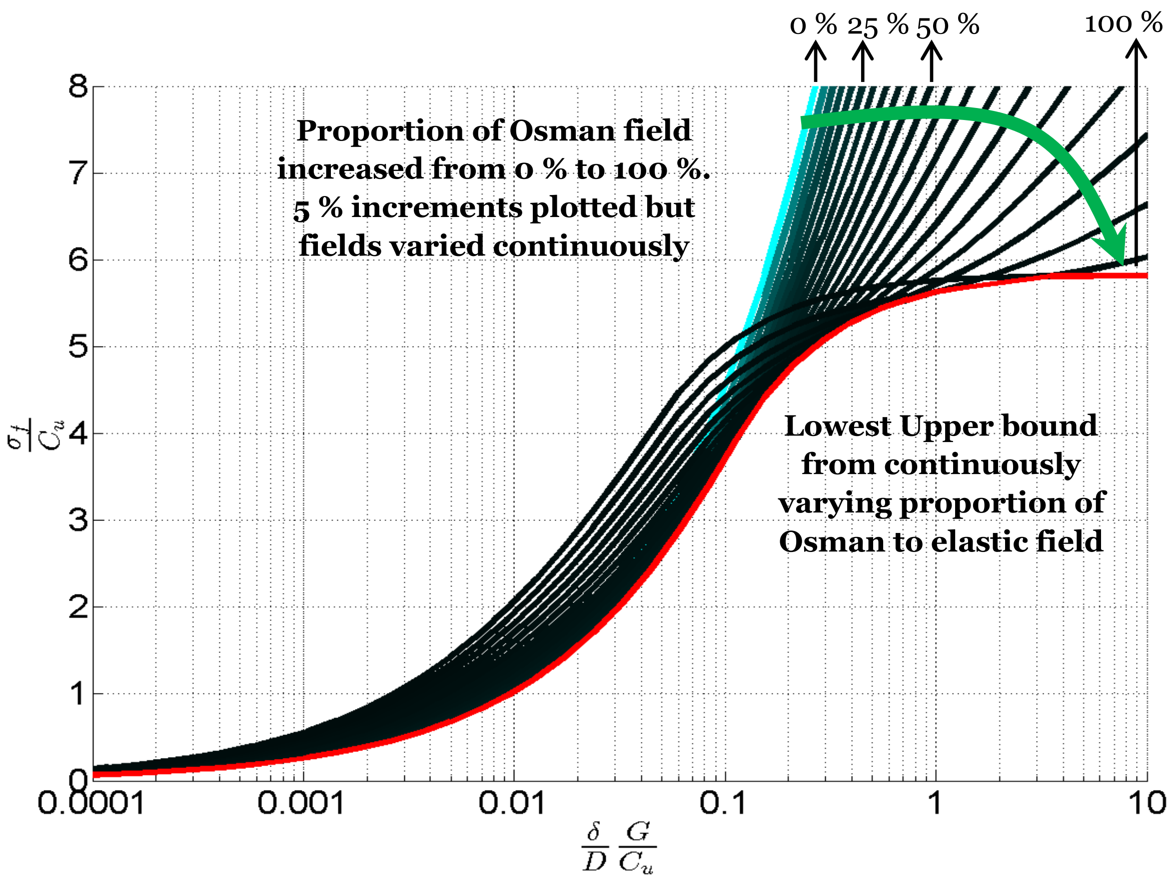

Figure 5-8: Continuously mixing elastic field and Osman field to produce optimal load-displacement behaviour beneath circular foundation

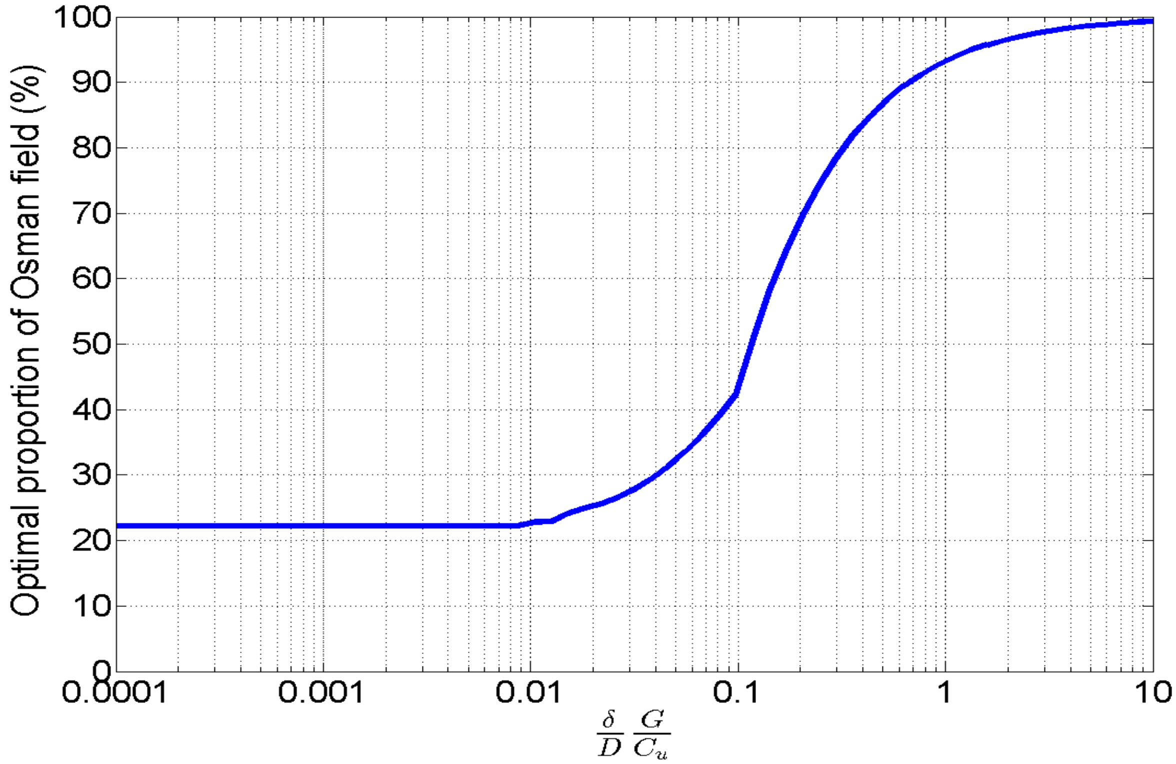

Figure 5-9: Determining proportion of Osman to elastic field to produce optimal deformation mechanism

Figure 5-10 illustrates a similar process but mixing the elastic field beneath a strip footing with the pure Prandtl field described earlier in Section 5.3.1. Whilst a trade-off can be observed, the initial response is dominated by mixes consisting of predominatly the elastic field with very low proportions of the pure Prandtl field. This compounds the earlier conclusion that whilst beneath a circular footing the rate of change of the deformation mechanism is quite rapid, resulting in the ULS deformation mechanism at low footing displacements, this appears not to be the case for strip footings.

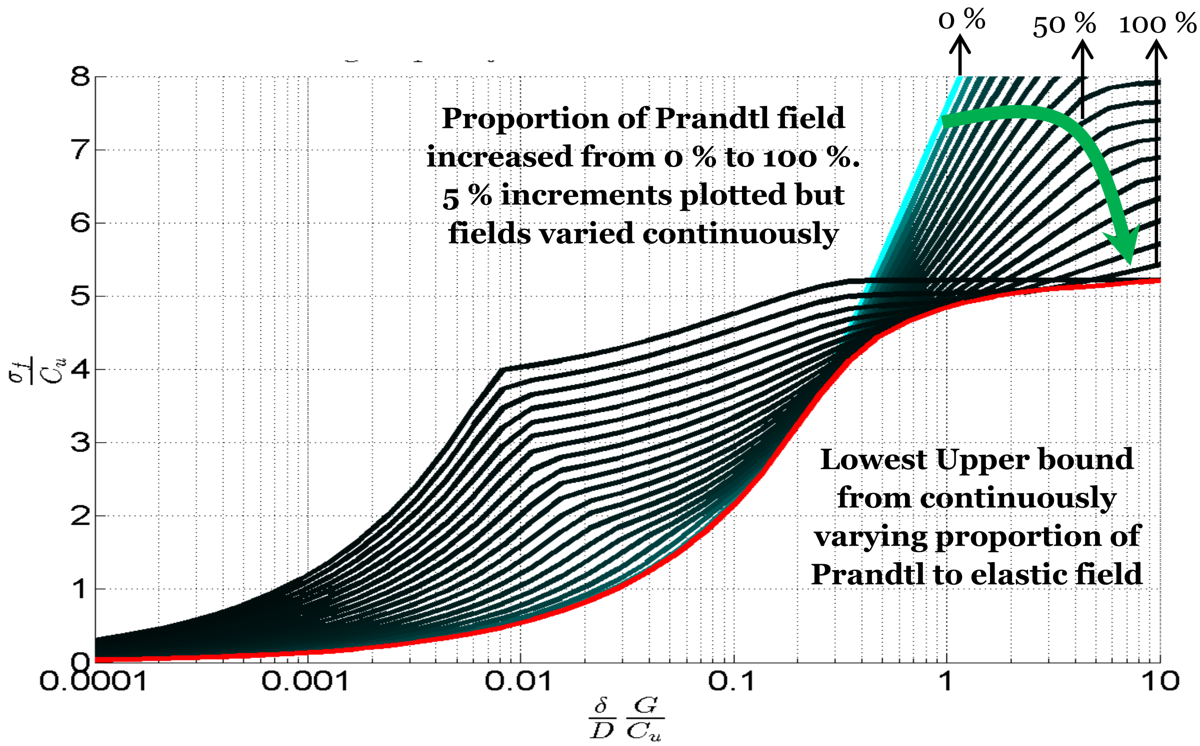

Figure 5-10: Mixing elastic field and pure Prandtl field to produce optimal load-displacement behaviour beneath strip foundation

5.3.1. Upper bound analyses for our GeoPIV fields

Of course, using the GeoPIV software we were able to observe the actual deformation mechanism that occurred beneath the footing. The original energy script (McMahon, 2013a) was modified by the author to allow the inputting of the experimentally observed GeoPIV data. We may hence calculate the complete load displacement behaviour for each inputted mechanism as if it occurred for all footing displacements.

Figure 5-11 illustrates this process for an intermediate mechanism beneath a circular shallow foundation. The individual plots have been previously explained in Section 5.3.1. Because we are directly using experimental measurements of the soil movements (rather than the mathematically defined fields previously used) the surfaces for the energy dissipated per unit area are somewhat more 'noisy'. Smoothing of the PIV data, as explained in Section 5.1, was used to mitigate for this. Further, the bulk of the energy dissipated for this intermediate mechanism is seen to occur within the expected soil regions and not dominated by the 'noise'. This improves our confidence in the load-displacement prediction.

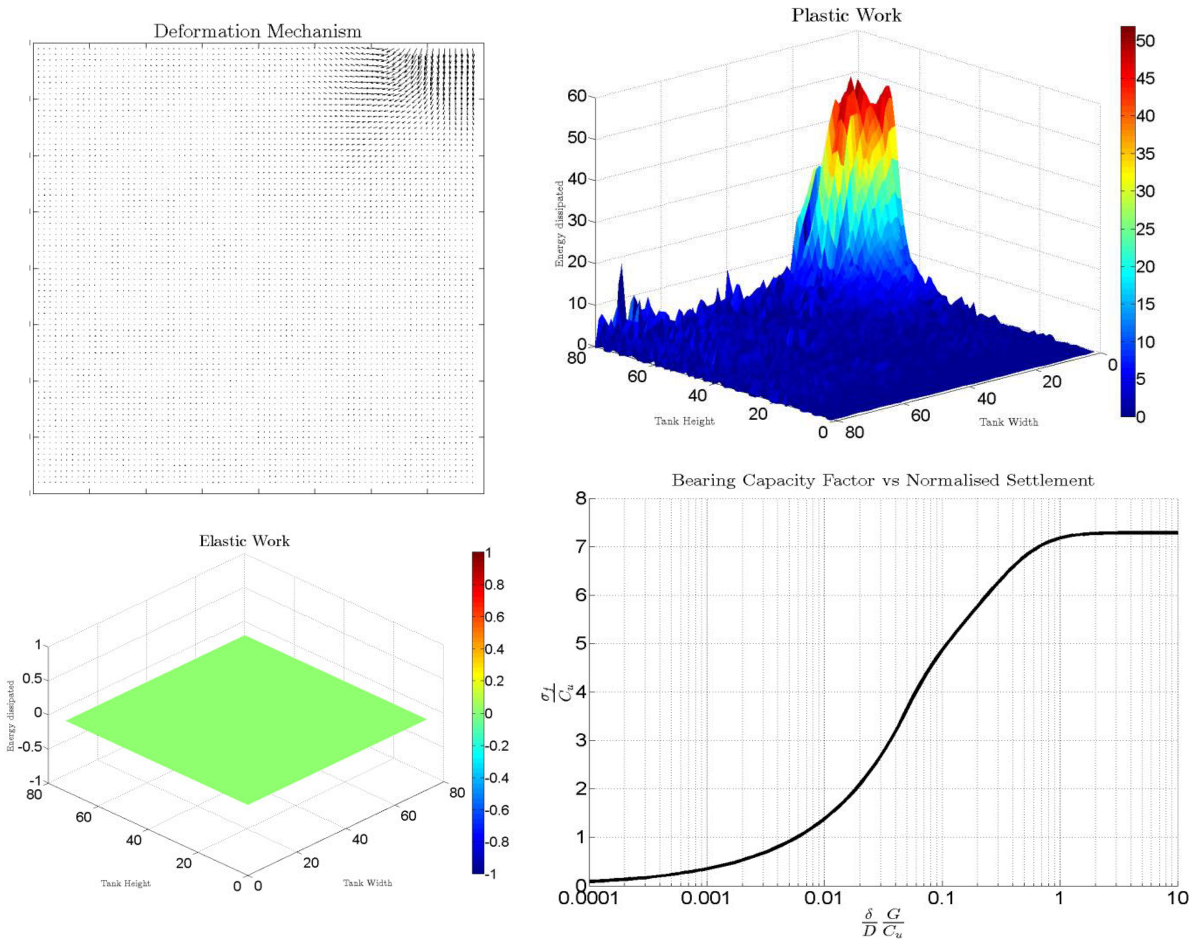

Figure 5-11: Using the modified energy script to calculate the load displacement behavior from the GeoPIV data from MSC1-b

In theory, this could be conducted for all recorded deformations in order to determine transition points between mechanisms and potentially match the experimentally measured load displacement behaviour. In practice, this procedure was found to work less well for earlier mechanisms. This is because the ratio of the energy dissipated throughout the mechanism to the 'noise' was smaller, and hence determining the true load-displacement behaviour would have required 'cleaner' GeoPIV results than those obtained.

Nevertheless, by running the procedure for numerous mechanisms and selecting the minimum values (as in Section 5.3.2 for the theoretical mixes) we can still obtain a relatively accurate estimate of the load-displacement behaviour implied by the GeoPIV results. This is shown in Figure 5-12, where the lighter lines indicate deformation mechanisms from lower footing displacements and vice versa. The transition between mechanisms is less obvious than for the idealised fields in Section 5.3.2, especially for the fields taken from low displacements of the footing.

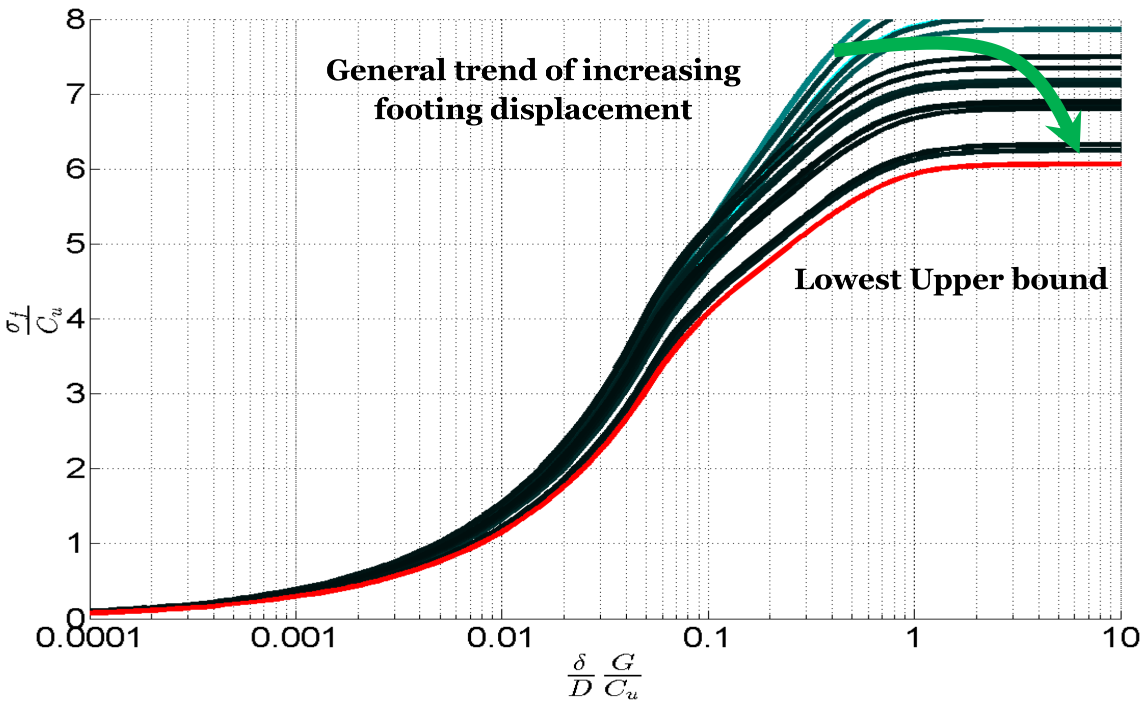

Figure 5-12: Using modified energy script to calculate the optimal load displacement behavior from the GeoPIV data from MSC1-b

5.3.2. Comparison of predictions

In the preceding sections we have obtained predictions of the load settlement behaviour using numerous different techniques, ranging from experimental measurements to purely theoretical predictions to mixtures of the two.

When considering the design implications of this work, we are clearly interested in which of these analytical methods is best able to predict the 'actual' load displacement behaviour (taken to be the average of the experimental observations, notwithstanding the limits of the experimental accuracy detailed in Section 5.2). To this end, Figure 5-13 and Figure 5-14 were produced.

The two figures reveal some interesting trends. Assuming the average of the experimentally observed results represents the 'actual' behaviour seems justified, as it is on the whole consistently lower than the theoretical and analytical predictions.

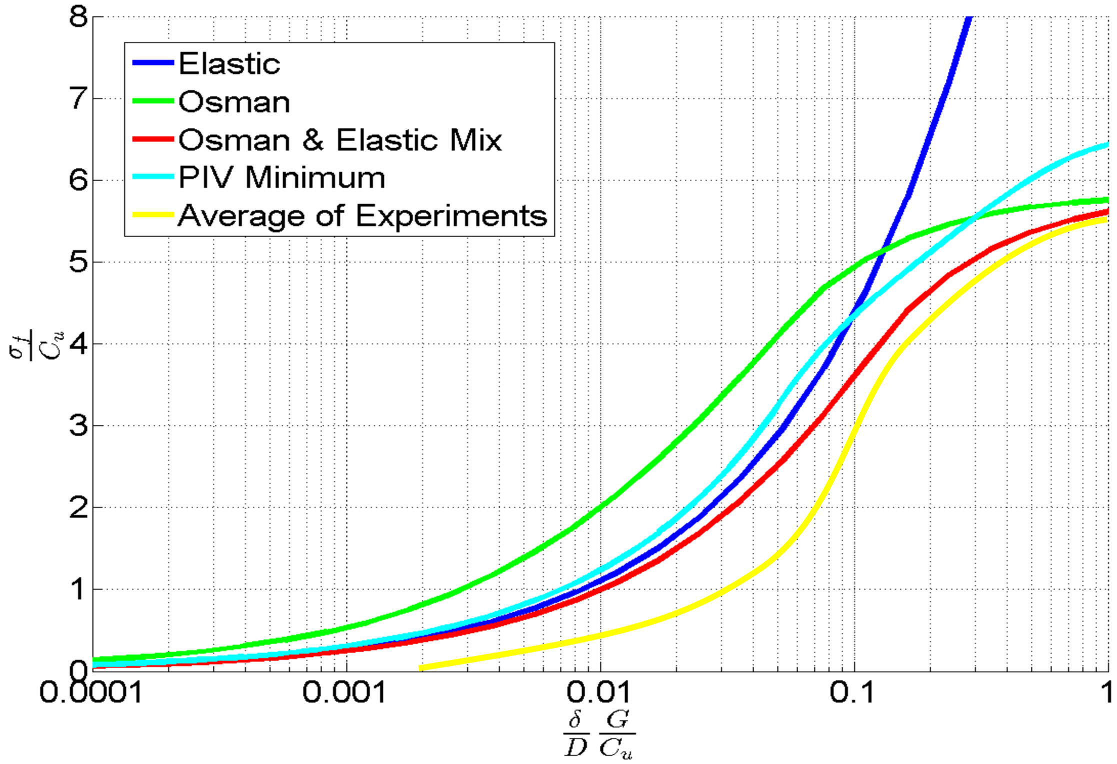

Figure 5-13: Comparing predictions and measurements of load-settlement behaviour beneath circular foundations

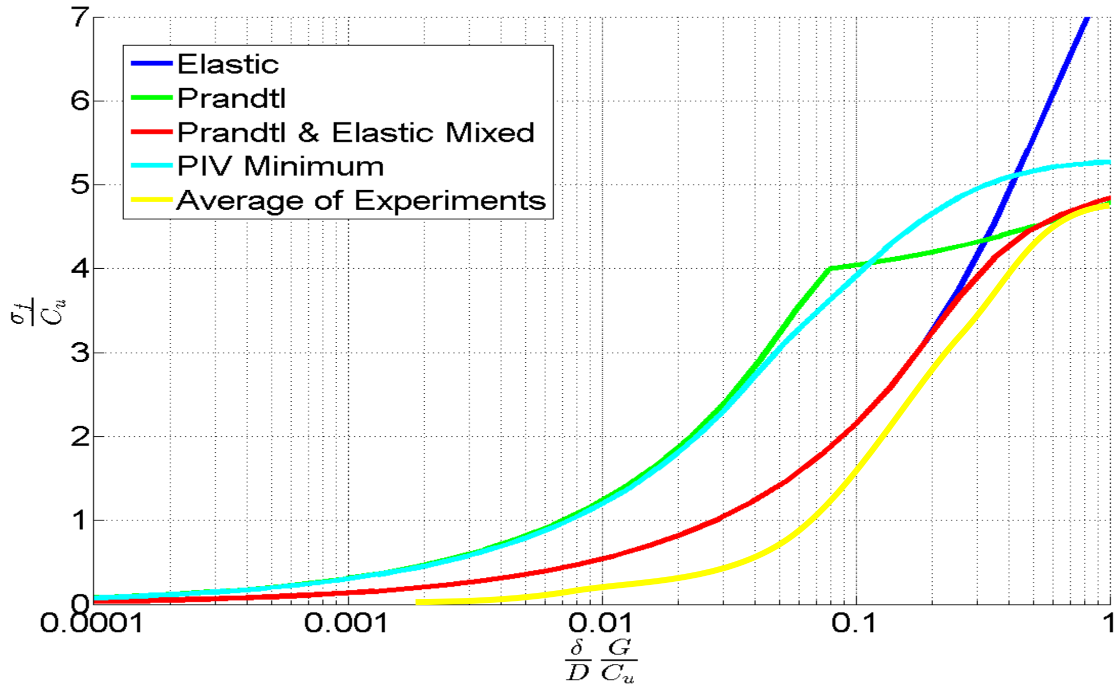

Figure 5-14: Comparing predictions and measurements of load-settlement behaviour beneath strip foundations

Concentrating first on the behaviour beneath the circular footing, the following conclusions can be drawn. Most of the applied methods are able to make reasonable predictions of the ULS load for the footing. The accuracy of the load settlement predictions is less consistent. Further, most methods are under predicting the settlement at any given load, which could well prove un-conservative for design.

The best prediction of load-settlement is produced by the mixing of the Osman and Elastic field. Except at very low levels of settlement, the match between the optimal mix of the idealised fields and the observed results is very good. Whilst the minimum of the GeoPIV results had the potential to match the experimentally observed load-settlement behaviour exactly, this was not realised. This is due to the fact mechanisms that could be successfully inserted tended to be from large displacements of the footing. This explains the increasingly close match between the 'PIV minimum' line and the measured results as the footing displacement increases. In order to achieve better results from the GeoPIV predictions, larger footings could be used to ensure the ratio of the footing displacements to the 'noise' in the soil mass is reduced.

Similar conclusions can be drawn from the strip footing results present in Figure 5-14. The mix between the pure Prandtl field and the elastic field matches well with average experimental results, whilst the other predictors match the ULS load but not the load-settlement behaviour. It is possible an even closer match between the mixed field and the experimental results could be realised. Instead of mixing the pure Prandtl mechanism with the elastic field a more optimal combination may be a mechanism with distributed plastic strains similar to the 'Osman field' (but that conserves volume under plane strain conditions) mixed with the elastic field.

The implications for design from these results may be profound. Whilst the ULS predictions from most methods are found to be satisfactory, the prediction of footing settlement under a given load can potentially be severely underestimated. Further, as Figure 5-14 and Figure 5-13 illustrate, the discrepancy between the experimentally observed and theoretical predictions of settlement is largest at the intermediate values of load. Typical factors of safety may be between 2 and 3, reducing the ULS load to exactly these intermediate values where purely plastic or elastic settlement estimates are worst. This will be further discussed in Section 6.

6. Concluding Remarks

This project has combined a variety of experimental and analytical techniques in order to investigate the deformation mechanism beneath shallow foundations. Due to the globally prolific use of shallow foundations, a view towards the practical implications for design has been maintained throughout. The following key conclusions can be drawn from the literature review, experiments performed and analytical work to date:

- The wide spread use of Shallow Foundations means that the optimisation between safety, performance and efficiency can have large scale ramifications in terms of socio-economic and environmental costs. There is hence a need to move away from satisfying the SLS requirements through arbitrary scaling down of the ULS loads. A more rationalised design approach was initially proposed by McMahon et al (2013a) and served as the catalyst for this project
- The visualisation of the deformation mechanisms beneath both circular and strip shallow foundations was successfully achieved using the GeoPIV software. The deformation mechanism was observed to change as the footing was loaded up to the ULS. This was true for both the circular and strip footing, although the rate of change of mechanisms was noted to be faster for the circular footing
- The mechanisms appeared to change almost continuously. There was an initial 'elastic' mechanism in which small, vertically downwards movements of a large amount of the soil mass accommodated the footing displacement without any 'heaving' at the soil surface. It was noted that this implies the soil was not behaving in a perfectly undrained manner, but it was also acknowledged that this would not be true in practice either. As the footing displacement increased, soil near the edges of the foundation moved horizontally outwards as well as vertically downwards. This can be well approximated by the cavity expansion model proposed by McMahon et al (2013a). At very large footing displacements (induced by loads above the usual design working loads of the footings) a 'Prandtl+' mechanism develops, in which the three zones predicted by Prandtl can be clearly identified as well as small movements of soil outside these regions
- Upper bound analyses provided further insight into the project, allowing comparison between the experimentally observed load-settlement behaviour and theoretically derived fields. The best match between the experimentally measured results and theoretical fields was achieved by mixing the elastic solution with the

Osman field for circular foundations and the pure Prandtl field for the strip foundations. The proportions of elastic field in the optimum mixes reflected the differing rate of change of deformation mechanisms beneath circular and strip foundations observed in the experimental results

- The practical implications of these findings may be profound. The changing deformation mechanism affects the load required to induce a given footing displacement. It is found that under typical 'working loads' for the footing the deformation mechanism is not well described by either purely elastic or purely plastic fields. This project highlights that knowledge of the changing deformation mechanism is necessary in order to accurately predict the settlement of the foundation at the working loads.

Potential future work:

- Improve the GeoPIV analysis to improve the prediction from the Upper bound method and the experimental measured results. This may require either more intelligent smoothing of the GeoPIV results (balance between smoothing out the 'noise' but not smoothing out peak values where they are valid) or repeat the experiments using larger footings or a higher resolution camera
- Assess whether similar results are obtained in different soil types. It would be interesting to see if finer grained clay that was more impermeable allowed the development of the 'elastic' type mechanisms observed. It was theorised this was only possible due to a small amount of densification of the soil
- Shallow foundations can potentially be loaded with combinations of vertical, horizontal and moment loads. Plasticity solutions for certain combinations, i.e. as proposed by Green (1954) for vertical and horizontal loading, also utilise the assumption of a rigid-perfectly plastic material. Similar experimental and analytical investigations to those performed in this report may facilitate more robust load-settlement predictions for combined loading of shallow foundations
- Indeed, the combination of using PIV to visualise deformation mechanisms and upper bound calculations based on the observed soil movements to allow rationalised load settlement predictions can be applied to numerous Geotechnical problems, ranging from shallow to deep foundations. Such methods may allow for increasingly technically justified designs that strike the balance between efficiency and safety that is required of the modern Geotechnical Engineer

References

Boussinesq, J. (1885). Application des potentiels a l'etude de l'equilibre et due movement des solids elastiques. Gauthier Villars, Paris

Carter, J. P. & Taiebat, H. A. (2000). Numerical studies of the bearing capacity of shallow foundations on cohesive soil subjected to combined loading. Géotechnique, 50(4), pp. 409–418. doi:10.1680/geot.2000.50.4.409

Carter, J. P. & Taiebat, H. A. (2010). A failure surface for circular footings on cohesive soils. Géotechnique, 60(4), pp. 265–273. doi:10.1680/geot.7.00062

Gourvenec, S. and Randolph, M. (2002). Effect of strength non-homogeneity on the bearing capacity of circular skirted foundations subjected to combined loading. In Proceedings of the 11th International Offshore and Polar Engineering Conference, pp. 693-698, Kyushu, Japan

Gourvenec, S. M., & Mana, D. S. K. (2011). Undrained vertical bearing capacity factors for shallow foundations, Geotechnique Letters, Vol. 1(4), pp. 101–108.

Green, A. P. (1954). The plastic yielding of metal junctions due to combined shear and pressure. Journal of the Mechanics and Physics of Solids, Vol. 2, pp. 189-211.

Hanselman, D.C. (2008). Improved 2D Streamlines. http://www.mathworks.co.uk/matlabcentral/fileexchange/38860-improved-2-d-streamlines/content/mmstream2.m. MATLAB Central File Exchange.

Houlsby, G.T. and Wroth, C.P. (1991). The Variation of the Shear Modulus of a Clay with Pressure and Overconsolidation Ratio. Soils and Foundations, Vol. 31, No. 3, September, pp. 138-143, ISSN 0038-0806

Klar, A., & Osman, A. S. (2008). Load – displacement solutions for piles and shallow foundations based on deformation fields and energy conservation. Géotechnique, 58(7), pp. 581–589. doi:10.1680/geot.2007.00128

MATLAB and Statistics Toolbox Release 2014a, The MathWorks, Inc., Natick, Massachusetts, United States

Meyerhof, G. G. (1951). The ultimate bearing capacity of foundations. Géotechnique 2(4), pp. 301-331.

McMahon, B. T., Haigh, S. K., and Bolton, M. D. (2013a), Cavity Expansion model for the bearing capacity and settlement of circular shallow foundations on clay, Géotechnique 63(9), pp. 746-752.

McMahon, B. T., Haigh, S. K., and Bolton, M. D. (2013b), Optimal displacement mechanisms beneath shallow foundations on linear-elastic perfectly plastic soil, Géotechnique 63(16), pp. 1447-1450.

Osman, A. S. & Bolton, M. D. (2005). Simple plasticity-based prediction of the undrained settlement of shallow circular foundations on clay. Géotechnique 55(6), pp. 435-447.

Prandtl, L. (1921). Uber die eindringungsfestigkeit plastischer baustoe und die festigkeit von schneiden. Zeitschrift fur Angewandte Mathematik und Mechanik, 1, pp. 15-20.

Skempton, A. W. (1951). The bearing capacity of clays. In Proceedings, Building Research Congress, volume 1, pp. 180-189. London, England.

Skempton, A. W. and Bjerrum, L. (1957). A contribution to the settlement analysis of foundations on clay. Géotechnique, 7(4), pp. 168-178.

Take, W. A., Bolton, M. D., & White, D. J. (2003). Soil deformation measurement using particle image velocimetry (PIV) and photogrammetry. Géotechnique, 53(7), pp. 619–631. doi:10.1680/geot.2003.53.7.619

Terzaghi, K. (1943). Theoretical Soil Mechanics. John Wiley & Sons, New York.

Vardanega, PJ & Bolton, MD (2012). Strength mobilization in clays and silts. Canadian Geotechnical Journal, 49, pp. 631-631.

Vardanega, PJ, Lau, BH, Lam, S, Haigh, S, Madabhushi, SPG & Bolton, MD. (2012). Laboratory measurement of strength mobilisation in kaolin: link to stress history. Geotechnique letters, Vol. 2, pp. 9-15.

White, D. J. and Take, W. A. (2002). GeoPIV: Particle Image Velocimetry (PIV) software for use in geotechnical testing. Technical report, CUED/D-Soils-TR322.

Appendix A: Mathematical Definition of the Osman field

Table A.1: Mathematical definition of the 'Osman field' following from Osman and Bolton (2005)

Zone	Radial displacement, u	Vertical displacement, v
Active zone	$\frac{-4\delta}{D^2}zr+\frac{2\delta}{D}r$	$\frac{4\delta}{D^2}z^2-\frac{4\delta}{D}z+\delta$
Fan zone	$\frac{V_1 r_1}{r}\frac{z}{\sqrt{\left(\frac{D}{2}-r\right)^2+z^2}}$	$\frac{V_1 r_1}{r}\frac{\left(\frac{D}{2}-r\right)}{\sqrt{\left(\frac{D}{2}-r\right)^2+z^2}}$
Passive zone	$\frac{1}{\sqrt{2}}\frac{V_2 r_2}{r}$	$-\frac{1}{\sqrt{2}}\frac{V_2 r_2}{r}$

$$V_1=4\sqrt{2}\left(\frac{r_1}{D}\right)^2\delta,\ r_1=\frac{D}{2}-\frac{1}{\sqrt{2}}\sqrt{\left(\frac{D}{2}-r\right)^2+z^2},\ V_2=4\sqrt{2}\left(\frac{r_2}{D}\right)^2\delta,\ r_2=\frac{3D}{4}-\frac{r}{2}-\frac{z}{2}$$

Appendix B: Risk Assessment Retrospective

The initial hazard assessment submitted was followed by submission of a full risk assessment due to the practical nature of the experiment and the location of the experimental work in a working laboratory. This was completed in consultation with Dr Stuart Haigh and was based of the safe systems of work already established at the Schofield centre. Specific hazards identified included:

- Heavy Lifting – Movement of the test rig and heavy experimental equipment was required. Safe lifting techniques were demonstrated in the Schofield centre induction day. Further, when it was deemed unsafe to conduct such tasks alone assistance from the technicians was sought or pallet trucks employed
- Moving parts – The 1D actuator featured moving parts however these were kept well away from any connecting cables and was operated remotely
- Electrical equipment – It was possible to only handle electrical equipment when the power supply was turned off and hence the risk of electrocution was minimised

Due to the detailed planning of experiments prior to conducting them, the hazards noted encompassed all those encountered during the course of the project. The value of detailed planning, both in terms of experimental accuracy and safety was a beneficial lesson resulting from the completion of the hazard and risk assessments.